JOURNAL OF GEOPHYSICAL RESEARCH: OCEANS, VOL. 118, 4600–4616, doi:10.1002/jgrc.20338, 2013

Atmospheric forcing intensifies the effects of regional ocean warming on reef-scale temperature anomalies during a coral bleaching event

Zhenlin Zhang,[1,2,3] James Falter,[1,2,3] Ryan Lowe,[1,2] Greg Ivey,[2,4] and Malcolm McCulloch[1,2,3]

Received 13 May 2013; revised 30 July 2013; accepted 5 August 2013; published 18 September 2013.

[1] We investigate how local atmospheric conditions and hydrodynamic forcing contributed to local variations in water temperature within a fringing coral reef-lagoon system during the peak of a marine heat wave in 2010–2011 that caused mass coral bleaching across Western Australia. A three-dimensional circulation model Regional Ocean Modeling System (ROMS) with a built-in air-sea heat flux exchange module Coupled Ocean Atmosphere Experiment (COARE) was coupled with a spectral wave model Simulating Waves Nearshore (SWAN) to resolve the surface heat exchange and wave-driven reef circulation in Coral Bay, Ningaloo Reef. Using realistic oceanic and atmospheric forcing, the model predictions were in good agreement with measured time series of water temperature at various locations in the coral reef system during the bleaching event. Through a series of sensitivity analyses, we found that the difference in temperature between the reef and surrounding offshore waters (ΔT) was predominantly a function of both the daily mean net heat flux ($\overline{Q_{net}}$) and residence time, whereas diurnal variations in reef water temperature were dependent on the diurnal fluctuation in the net heat flux. We found that reef temperatures were substantially higher than offshore in the inner lagoon under normal weather conditions and over the entire reef domain under more extreme weather conditions (0.7°C–1.5°C). Although these temperature elevations were still less than that caused by the regional ocean warming (2°C–3°C), the arrival of peak seasonal temperatures in the summer of 2010–2011 (when net atmospheric heat fluxes were positive and abnormally high) caused substantially higher thermal stresses than would have otherwise occurred if offshore temperatures had reached their normal seasonal maxima in autumn (when net atmospheric heat fluxes were negative or cooling). Therefore, the degree heating weeks calculated based on offshore temperature substantially underestimated the thermal stresses experienced by the reef in the period leading up to the observed bleaching event (3 versus 11°C-weeks).

Citation: Zhang, Z., J. Falter, R. Lowe, G. Ivey, and M. McCulloch (2013), Atmospheric forcing intensifies the effects of regional ocean warming on reef-scale temperature anomalies during a coral bleaching event, *J. Geophys. Res. Oceans*, *118*, 4600–4616, doi:10.1002/jgrc.20338.

1. Introduction

[2] Over the past few decades, coral reefs worldwide have been subjected to an increasing frequency and severity of mass bleaching events as a result of ongoing anthropogenic climate change [*Donner et al*., 2007, 2009; *Hoegh-Guldberg*, 1999; *Sheppard*, 2003]. It is widely acknowledged that thermal stress is the major cause of these observed bleaching events around the globe [*Spalding*, 2009; *Wooldridge and Done*, 2004]. Typically, bleaching is caused when corals are exposed to prolonged thermal stress in the form of persistent, abnormally high sea surface temperature (SST) over the course of several weeks to months [*Berkelmans*, 2009; *Frieler et al*., 2010; *Heron et al*., 2012; *Manzello et al*., 2007; *Strong et al*., 2011]. However, the likelihood and intensity of bleaching at a given reef location is additionally influenced by the local range of water temperatures to which corals have historically been

Additional Supporting Information may be found in the online version of this article.

[1]School of Earth and Environment, The University of Western Australia, Perth, Western Australia, Australia.
[2]The UWA Oceans Institute, The University of Western Australia, Perth, Western Australia, Australia.
[3]ARC Centre of Excellence for Coral Reef Studies, The University of Western Australia, Perth, Western Australia, Australia.
[4]School of Environmental Systems Engineering, The University of Western Australia, Perth, Western Australia, Australia.

Corresponding author: Z. Zhang, School of Earth and Environment, The University of Western Australia (M004), 35 Stirling Highway, Crawley, Perth, WA 6009, Australia. (zhenlin.zhang@uwa.edu.au)

2169-9275/13/10.1002/jgrc.20338

exposed [*Miller et al*., 2011]. For example, corals which have been previously exposed to higher water temperature can be more resilient to future thermal stress events and, therefore, less likely to bleach under the same conditions [*Carilli et al*., 2012; *Castillo et al*., 2012; *Cook et al*., 1990; *Sammarco et al*., 2006; *Ware et al*., 1996]. Thus, bleaching between and within reef systems may exhibit a large degree of variability, depending on the magnitude and duration of deviations from "normal patterns" of SST [*Berkelmans et al*., 2004; *Glynn*, 1993; *Hoegh-Guldberg and Salvat*, 1995; *Lenihan et al*., 2008; *Nadaoka et al*., 2001; *West and Salm*, 2003]. Previous studies have shown that during the day the temperature of reef waters can be several degrees warmer than offshore as a result of local heating [*Castillo and Lima*, 2010; *Davis et al*., 2011; *Jokiel and Brown*, 2004; *Wells et al*., 2012]. Therefore, to better understand the thermal stress that reefs are exposed to during a given period of offshore warming, we must better understand and predict how local atmospheric heat exchange combined with reef circulation influence the in situ temperature of reef waters.

[3] There are a number of factors that can drive local variations in the temperature of reef waters; however, each of these factors usually falls into one of the three groups [*Jokiel and Brown*, 2004; *Obura*, 2005; *Sheppard*, 2003; *West and Salm*, 2003; *Yee et al*., 2008]. The first group includes factors related to atmospheric conditions such as light, cloud cover, aerosol composition and abundance, wind speed, relative humidity (RH), and air temperature; all of which influence heat exchange at the air-sea interface [*Gill et al*., 2006; *Glynn*, 1993; *Mumby et al*., 2001; *Smith*, 2001]. The second group includes factors related to oceanic conditions, such as wave forcing, tidal elevation, and offshore geostrophic flow that influence the residence times (and therefore heat accumulation) of waters across a given reef system [*Coronado et al*., 2007; *Davis et al*., 2011; *Franklin et al*., 2013; *McCabe et al*., 2010; *Zhang et al*., 2011, 2012]. The temperature gradient between a reef and adjacent ocean as well as within the reef system can also cause buoyancy-driven flow that results in further exchange of heat across the reef system [*Monismith et al*., 2006]. The third group includes factors related to the morphology of the reef system itself, as well as that of the extended continental shelf surrounding reef systems. The strength and pattern of circulation (and therefore the heat fluxes) that a particular reef system experiences under a given set of hydrodynamic conditions is strongly dependent on the local- and system-scale morphology of that system [*Falter et al*., 2013; *Lenihan et al*., 2008; *Lowe et al*., 2010, 2009; *Zhang et al*., 2012].

[4] Previous studies of temperature-driven bleaching typically assessed local thermal stress conditions through statistical approaches combining local environmental factors (e.g., cloud cover, wind speed, surface currents, etc.) with large-scale (~10s of km) regional SST data obtained from satellites [*Maina et al*., 2008; *McClanahan et al*., 2007; *Wooldridge and Done*, 2004; *Yee et al*., 2008]. While such approaches have been effective in identifying the qualitative influence of local environmental factors on bleaching at a particular reef during a particular event, it is difficult to extrapolate the results of such studies to a wider range of reef systems and climate conditions given their inherent empirical basis. Thus, a more fundamentally mechanistic approach based on the physics governing air-sea heat exchange and the circulation of reef waters is required to more realistically predict the local variations in water temperature for different reef systems under different climate scenarios. Recent efforts have shown how diurnal changes in local water temperatures at specific reef sites spanning hundreds of meters could be explained through such fundamental, mechanistic relationships [e.g., *Davis et al*., 2011; *McCabe et al*., 2010]. Here we use a hydrodynamic-thermodynamic model to simulate the combined effect of wave-driven transport and atmospheric heating on fine-scale temperature variations across a coastal reef-lagoon system covering ~10 km^2. Through the use of a numerical model we can resolve changes in the temperature of reef waters at relatively high spatial resolution (tens of meters) and temporal resolution (minutes to hours) using input from larger, regional- and global-scale databases on ocean temperature [*Chao et al*., 2009; *Eidenshink and Faundeen*, 1994; *Strong et al*., 2011]. Analogous numerical modeling approaches have been successful in simulating spatial and temporal variability in water chemistry at the scale of individual reef systems [*Falter et al*., 2013; *Zhang et al*., 2011, 2012]. Such models have also been used to simulate the influence of tidal flushing on diurnal changes in water temperature within an idealized reef lagoon; albeit in the absence of wave forcing [*McCabe et al*., 2010].

[5] The first aim of the present study is to develop and validate a coupled hydrodynamic-thermal numerical model by simulating local variations in water temperature across a fringing reef-lagoon system. The second aim is to explore the particular sensitivity of water temperatures within the reef system to a variety of oceanic and atmospheric forcing mechanisms. The final aim of the study is to investigate how local oceanic and atmospheric forcing contributed to observed elevations in local reef water temperatures and thermal stresses during a regional marine heat wave that struck Ningaloo Reef in the austral summer of 2010–2011 [*Feng et al*., 2013; *Pearce and Feng*, 2012]. During this event, offshore temperatures reached levels 2–3°C above their climatological average and unprecedented mass coral bleaching was observed across the entire Ningaloo Reef system [*Depczynski et al*., 2013; *Moore et al*., 2012]. We therefore focused our attention on the period leading up to and following the reported mass bleaching at Ningaloo.

2. Methods

2.1. Study Site and Field Experiment

[6] Our study site was Coral Bay (23.15°S; 113.74°E), a fringing coral reef-lagoon system in the southern region of the World Heritage Ningaloo Reef in Western Australia (Figure 1a). Coral cover throughout the bay is extensive, ranging from around 40% inside the lagoon to nearly 90% at the outer reef margin, with a wide range of species, but with coral cover mainly dominated by the genera *Acropora* and *Montipora* [*Cassata and Collins*, 2008; *Simpson et al*., 1993]. Previous studies at this study site have shown that spatial patterns in currents and water chemistry are predominantly controlled by wave forcing [*Zhang et al*., 2011, 2012].

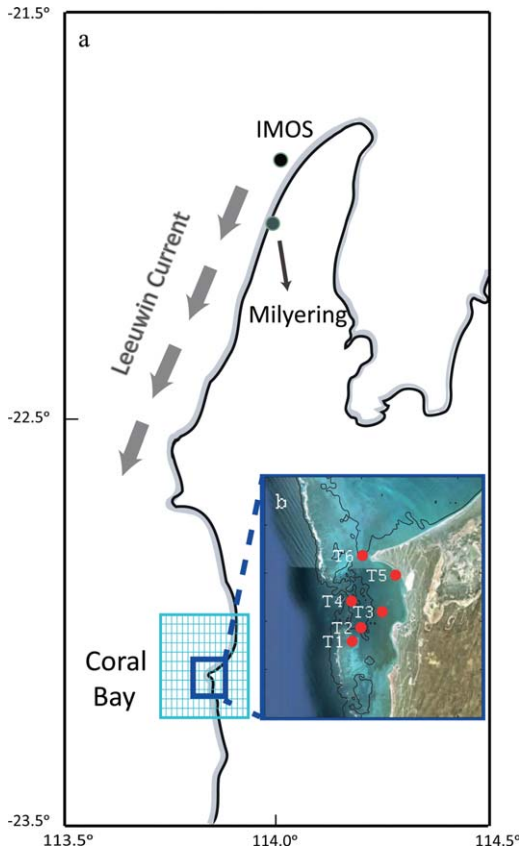

Figure 1. (a) Geographic location of the study site at Coral Bay and (b) study sites and instrument locations within Coral Bay. The mesh in Figure 1a denotes the computational domain. The black contour lines show 4 m isobath. Long-term near-surface water temperatures were measured at IMOS (Integrated Marine Observation System: http://www.imos.org.au/) site to calibrate with the remote-sensed SST; Milyering indicates the location of the nearest weather station on the Ningaloo Reef Shelf.

[7] Water temperatures within Coral Bay were measured in situ with six temperature loggers (Hobo Pro-v2 U22, Onset; ±0.2°C accuracy) positioned at the back reef flat (T1), in the lagoon (T2, T3, and T5), and in the two channels (T4 and T6) from mid-February 2011 to June 2012 to document both the spatial and temporal variation of water temperatures in Coral Bay (Figure 1b). However, in the present paper, we only focus on the period from January through February 2011, when record-high temperatures and coral mass bleaching occurred (with nearly 30% of the total coral coverage being affected) [*Moore et al*., 2012]. The mean water column depths of the sampling points (from T1 to T6) were 2.5, 5, 2.5, 7, 1.5, and 7 m, respectively. The temperature loggers were deployed (from T1 to T6) at depths of approximately 2, 3, 1.5, 6.5, 1.5, and 6.5 m, respectively (or 0–2 m off the bottom) and sampled every 5 min.

[8] Daily offshore SSTs were obtained from Group for High-Resolution Sea Surface Temperature (GHRSST) global Level 4 SST products provided by NOAA/National Climatic Data Center prior to 2010 and G1SST (Global 1-km Sea Surface Temperature) provided by NASA Jet Propulsion Laboratory from January 2010 onward. The GHRSST is provided at 25 km resolution and uses optimal interpolation (OI) to blend SST data mainly from Advanced Very High Resolution Radiometer (AVHRR) with in situ measurements [*Reynolds et al*., 2007]; whereas G1SST is provided at 1 km resolution and uses a two-dimensional variational data assimilation method to blend satellite images from AVHRR as well as from a few other satellite products (e.g., MODIS, GOES imager, etc.) [*Chao et al*., 2009]. A comparison between the two SST products and temperature mooring data obtained from an Integrated Marine Observation System (IMOS; http://www.imos.org.au/) site on the northern end of Ningaloo Reef (21.87°S, 113.95°E; see Figure 1a) at 17 m depth over a full year showed that both satellite data sets agreed very well with the in situ measurements ($r^2 \geq 0.9$, $rmse < 0.8$°C), with the G1SST showing slightly better match with the mooring data than GHRSST (Figure 2).

2.2. Numerical Models

[9] To simulate the wave-driven circulation and heat budget in Coral Bay, we used the three-dimensional Regional Ocean Modeling System (ROMS, version 3.6) [*Shchepetkin and McWilliams*, 2005] two-way coupled to the spectral wave model SWAN (Simulating Waves

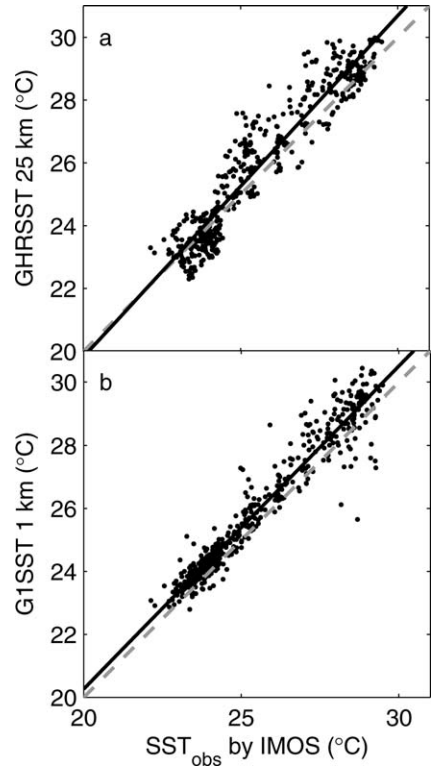

Figure 2. Observed sea surface temperature (SST) derived from the offshore IMOS mooring observed at 17 m depth (21.87°S, 113.95°E) versus global daily blended satellite SST for the period between 2 August 2010 and 6 November 2011 at (a) 25 km resolution (GHRSST) and (b) 1 km resolution (G1SST). The regression lines (in black) for the two SST products are: $SST_{sat} = 1.086 \times SST_{obs} - 1.9$ ($r^2 = 0.90$, $rmse = 0.74$°C, $n = 453$) for GHRSST and $SST_{sat} = 1.025 \times SST_{obs} - 0.7$ ($r^2 = 0.92$, $rmse = 0.57$°C, $n = 453$) for G1SST, respectively. The gray dashed lines denote the 1:1 lines.

Table 1. Configurations of the Hindcast and Scenario Simulations[a]

Simulations	No.	Variable	Value	Default Value	Unit
Hindcasts	1	All	Default		
	2 and 3	Albedo	0.08, 0.20	0.14	
	4 and 5	Relative humidity	50%, 95%	Time varying (~80%)	
Scenarios	1	All	Default		
	2–5	Daily mean of Q_{net}	150, 0, −75, −200	75	W m^{-2}
	6 and 7	Amplitude of Q_{net}	910, 390	250	W m^{-2}
	8–10	Wave height	1, 3, 4	2	m
	11 and 12	Wave period	8, 16	12	s
	13	Alongshore current	Northward	Southward	

[a]The order of the simulation numbers corresponds to the order of the values listed.

Nearshore, version 40.51) [*Booij et al*., 1999]. We also activated the air-sea interaction module COARE (Coupled Ocean Atmosphere Experiment) bulk algorithm [*Fairall et al*., 2003] in ROMS to calculate air-sea heat exchanges at each time step. To account for wave setup and wave-driven flow, this version of ROMS uses the wave-current interaction formulations of *Mellor* [2003] to calculate radiation stresses. Although different wave-current interaction algorithms exist to parameterize the vertical depth-dependent distribution of radiation stresses, these detailed effects are generally not important for predicting the overall depth-averaged wave forces in the surf zones of shallow water systems [*Kumar et al*., 2012]. We used the same computational grid (488 × 600 grid cells, 50 m grid size, and four vertical layers), domain (see Figure 1a), time step (2 s), and the configuration as in the hydrodynamic models described by *Zhang et al*. [2012], where further details of model domain, settings, and validation with hydrodynamic observations are given. A higher vertical resolution was not required as the water column for the shallow reef domain is mostly well mixed due to the combined effects of the generally strong wave forcing (>1 m), shallow water depth (<5 m), and high bottom roughness (~0.02 m) at this site [*Zhang et al*., 2012]. This can be illustrated by a simple estimation of the horizontal distance the flow travels before an initially thermally stratified water column becomes completely well mixed using an integral mixed-layer model as described by *Ivey and Patterson* [1984] and *Niller* [1975].

[10] At each time step, the COARE algorithm calculated the rate of change of water temperature (T) due to air-sea heat fluxes (Q_{net}) within the computational cells as

$$\frac{\mathrm{d}T}{\mathrm{d}t} = \frac{Q_{net}}{\rho_w C_p h} \tag{1}$$

where ρ_w is the water density, C_p is the specific heat of air, and h is the water depth. Here Q_{net} is the net heat flux across the air-sea interface (positive values represent the net transfer of heat to the ocean), which is the sum of four water-surface heat flux terms, i.e.:

$$Q_{net} = Q_{sd}(1-\gamma_S) + (Q_{ld} - Q_{lu}) + Q_{lt} + Q_{sb} \tag{2}$$

where Q_{sd} is the downward shortwave radiation at the water surface, γ_S is the total albedo (including both surface and bottom albedo), Q_{ld} and Q_{lu} are the downward and upward longwave radiation, Q_{lt} is the latent heat flux, and Q_{sb} is the sensible heat flux. Our estimate of bottom albedo includes radiation absorbed by both the water column and benthos, and we assume that all radiation absorbed by the benthos contributes to heating of the entire water column (Appendix A). Q_{lt} and Q_{sb} can be calculated by bulk atmospheric heat flux parameterizations as [*Geernaert et al*., 1987]:

$$Q_{lt} = \rho_{air} L_v C_w U_{10}(q_{10} - q_s) \tag{3}$$

$$Q_{sb} = \rho_{air} C_p C_H U_{10}(T_{air} - T_s) \tag{4}$$

where ρ_{air} is the air density, L_v is the latent heat of vaporization, U_{10} is the wind speed at 10 m above the water surface, q_{10} is the specific humidity at 10 m above the water surface, q_s is the saturated specific humidity at the water surface, T_{air} is the air temperature at 10 m above the water surface, T_s is the water surface temperature, and C_w and C_H are the heat exchange coefficients, which are functions of sea surface roughness [*Fairall et al*., 2003]. This modified water temperature field is then fed back into ROMS, where the transport and turbulent diffusion of heat are subsequently computed.

[11] We first ran hindcast simulations (Hindcasts 1–5; Table 1) of circulation and net heating in Coral Bay over a 2 week period following the mass bleaching event when in situ observed temperatures first became available (15 February to 1 March 2011 [*Moore et al*., 2012]). To drive the model, we used local atmospheric variables (shortwave radiation, air temperature, relative humidity, etc.) as well as tide and wave forcing conditions supplied from global databases (see section 2.3). We assumed a constant southward alongshore current equal to the measured monthly averaged Leeuwin Current (~0.1 m s^{-1}) recorded in this region during a prior summer [*Smith et al*., 1991]; however, we will show later in section 3.3 that water temperatures in Coral Bay were relatively insensitive to the magnitude of the alongshore current. Although G1SST provided a reliable historical record and the long-term trend of SSTs offshore (Figure 2b), the day-to-day variation in offshore SSTs in this region contained an estimated error of ~1°C (output from G1SST). Given that the daily SST product alone would provide an inadequate boundary condition for our computational domain, we used the daily average temperature measured at T1 to adjust the upstream temperature boundary condition. We then focus on the residual diurnal temperature variations at T1 $\left(T(t) - \overline{T}_{24}\right)$ as well as

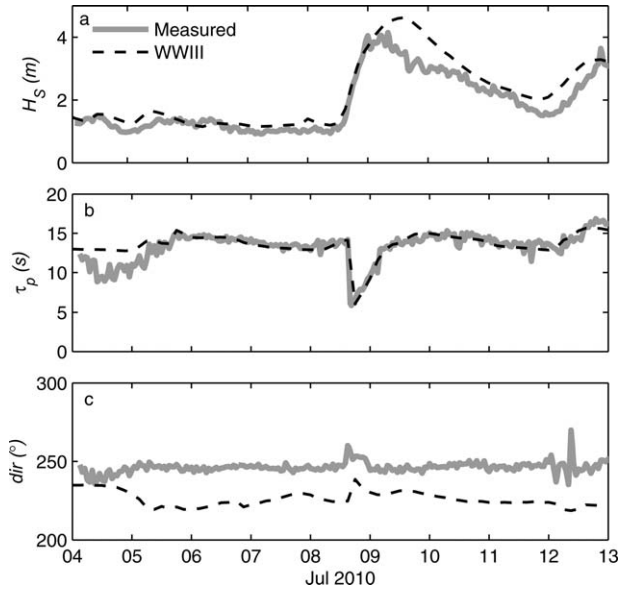

Figure 3. Verification of the (a) significant wave height, (b) wave direction (clockwise from true north), and (c) peak period modelled by WWIII with those measured at a forereef mooring site (113.7443°E, −23.149°N) at Coral Bay for the period between 4 and 13 July 2010.

the observed temperature data from all other sites (T2–T6) to independently validate the model. We used a spatially averaged total albedo in the default simulation (Hindcast 1: $\gamma_S = 0.14$) similar to that reported by *Davis et al.* [2011]; however, we also tested the sensitivity of the hindcast model to a realistic spatial range of total albedos in Hindcast 2 and Hindcast 3 (γ_S= 0.08, 0.20; see Table 1 and Appendix A). As latent heat flux (evaporative cooling) was the major term in the outgoing heat fluxes, two more simulations were conducted to investigate the sensitivity of the hindcast model to relative humidities (RH) as low as 50% (Hindcast 4) and as high as 95% (Hindcast 5), given a time-varying RH fluctuating around the mean of ∼80% during the simulation period (see section 3.1). These values represented end members bounding 95% of the observed range of RH for Coral Bay during the summer over the past 20 years (mean RH = 70%).

[12] We next ran a series of scenario tests (Table 1), each with constant hydrodynamic forcing and an idealized diurnal heating pattern and perturbing from the central case (Scenario 1) by changing one forcing variable, to investigate the general effect of varying the total net heat flux and wave forcing on the resulting spatial and temporal patterns of reef water temperatures in Coral Bay. While there are a number of different atmospheric variables that influence the net flux of heat across the air-sea interface (e.g., light, cloud cover, relative humidity, wind speed, air temperature, albedo, etc.), we are primarily interested in simply comparing the relative importance of wave-driven circulation versus total atmospheric thermal forcing on spatial and temporal deviations in the temperature of reef water relative to offshore. Therefore, we evaluated the sensitivity of the Coral Bay reef-lagoon system to variations in the defined total daily net heat flues ($\overline{Q_{net}}$) rather than the multitude of individual atmospheric forcing terms which contribute both positively and negatively to $\overline{Q_{net}}$. For the scenario tests, surface heating was confined to the Coral Bay reef-lagoon domain (Figure 1b) to focus our sensitivity analysis only on reef-scale thermal forcing rather than on variations in mixed-layer dynamics offshore. To constrain the range of the forcing and heating conditions chosen, we used historical summer data (see section 2.3) collected over the preceding 20 years (January through March from 1990 to 2010). Forcing for the default simulation (Scenario 1) was determined from the mean summer condition over this 20 year period, i.e., a constant offshore significant wave height of 2 m, a peak wave period of 12 s, a uniform northward wind of 6 m s^{-1}, a constant southward alongshore current of 0.1 m s^{-1} [*Zhang et al.*, 2012], and a recurring diurnal heat flux with a daily average of +75 W m^{-2} and daily amplitude (max – min) of 650 W m^{-2}. We further assumed that diurnal net heat fluxes varied sinusoidally during the day and were constant at night.

[13] Scenarios 2–7 tested the response of water temperature to a range of changing daily net heat fluxes; a range that covered 90% of all days for the entire year. Scenarios 8–10 investigated the effect of changing offshore wave height from 1 to 4 m and Scenarios 11–12 investigated the effect of changing peak wave period from 8 to 16 s, which also covered more than 90% of wave forcing conditions recorded at Coral Bay for the entire year. Finally, Scenario 13 tested the effect of the alongshore current direction (northward versus southward). For all the scenario tests, a constant SST of 28.5°C at the lateral boundaries was applied to replicate the mean offshore SST during the period of mass bleaching (late January to early February 2011). All test simulations were run for 6 days, given that a quasi-equilibrium diurnal curve of water temperature could be obtained by the third day following this initial spin-up period.

2.3. Model Inputs

[14] To simulate the circulation within Coral Bay, the ROMS-SWAN model requires offshore (incident) significant wave height, wave direction, peak wave frequency, tidal constituents, wind, and alongshore current as model inputs. The incident wave heights and peak wave frequencies were provided by the global hindcast reanalysis product of the NOAA WaveWatch III (WWIII) model (polar.ncep.noaa.gov/waves), which has a spatial resolution of 0.5° and a temporal resolution of 2 h [*Tolman and Chalikov*, 1996; *Tolman et al.*, 2002]. Wave data from WWIII were validated against the measured wave conditions at a forereef site off Coral Bay (113.7443E, 23.149S) during a priori 10 day field experiment in 2010 [*Zhang et al.*, 2012], as no offshore wave measurements were available during the hindcast simulation period. Comparison between measured wave and output from the WWIII data off Coral Bay showed good agreement for both significant wave height and peak frequency (Figures 3a and 3b). The comparison of wave direction showed a roughly 20° difference between the two (Figure 3c), likely due to the effect of refraction given the local depth (∼12 m) where the field observations were made on the forereef, i.e. the WWIII wave directions would reflect those offshore in deep water. Prior measurements have shown that wave directions at the forereef were nearly constant at 244 ± 5° for more than

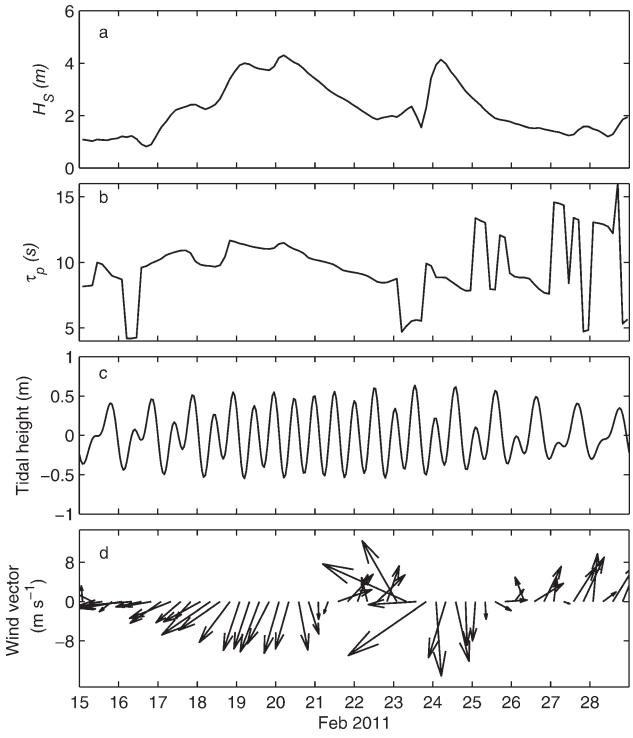

Figure 4. Hydrodynamic forcing conditions between 15 February and 1 March 2011 at Coral Bay. (a) Significant wave heights predicted from WWIII, (b) peak surface wave periods predicted from WWIII, (c) tidal heights from OTIS, and (d) wind vectors from CFSRV2.

80% of the time (Figure 3c). We therefore assumed a constant wave direction of 244° during the hindcast period. To simulate tidal forcing, we used the OTIS (OTIS is the OSU Tidal Inversion Software, where OSU stands for Oregon State University) [*Egbert et al.*, 1994] to extract the first eight tidal harmonic constituents (M2, S2, N2, K2, K1, O1, P1, and Q1) from the OTIS Indian Ocean Tidal Solution (http://volkov.oce.orst.edu/tides/IO.html) and applied them to the lateral boundaries of the computational domain.

[15] To calculate air-sea heat and momentum fluxes, a number of variables (wind speed, downward shortwave radiation, net longwave radiation, air temperature, relative humidity, total albedo, and atmospheric pressure) were required as model inputs (see equations (1)–(4)). Data for these atmospheric variables were provided by the NCEP Climate Forecast System Reanalysis Version 2 (CFSRV2) product (http://cfs.ncep.noaa.gov/cfsr/), which has a 0.2° grid resolution and a minimum time interval of 1–6 h (depending on the variables) for the whole globe [*Saha et al.*, 2010]. Because shortwave radiation output from CFSRV2 was provided only four times a day before March 2011, and therefore incapable of reproducing the true diurnal cycle of radiative forcing at Coral Bay, we used the photosynthetically active radiation (PAR) recorded half hourly from a weather station on the Ningaloo coast north of the study site at Milyering (22.03°S, 113.92°E; see Figure 1a) maintained by Australian Institute of Marine Science. The measured PAR (in μmol s^{-1} m^{-2}) was then converted to half-hourly surface shortwave radiation (Q_{sd} in W m^{-2}) based on a linear regression between the measured PAR and the forecast downward shortwave radiation at the times of the day when data was available from CFSRV2 during the months around the bleaching event (from 1 December 2010 to 31 March 2011), i.e., $Q_{sd} = 0.32$ PAR + 10 ($r^2 = 0.9$, $p < 0.05$, $n = 484$).

3. Results

3.1. Field Observations and Local Forcing

[16] During the 2 week period covered by the hindcast simulations (15 February through 1 March 2011), significant wave heights offshore of Coral Bay varied between 1 and 4 m (Figure 4a), peak wave period varied between 4 and 16 s (Figure 4b), tidal elevations varied within the range of ±0.6 m (Figure 4c), and wind speeds reached up to 10 m s^{-1}, switching between northerly and southerly directions (Figure 4d). Net heat fluxes across the air-sea interface followed a quasi-sinusoidal pattern during the day and were negative at night (Figures 5a and 5b). The diurnal amplitude of the net heat flux was generally between 600 and 700 W m^{-2}, except on February 23 when it was just 320 W m^{-2} due to the presence of high cloud cover on that day (indicated by a substantial drop in shortwave radiation; see Figure 5a). During the model hindcast period, the dominant terms in the heat flux budget were the shortwave radiation (daily mean = 240 W m^2) and latent heat flux terms (daily mean = −150 W m^2), while the net longwave and sensible heat flux terms were far lower in magnitude (daily mean = −22.6 and 0.6 W m^{-2}, respectively). The relative

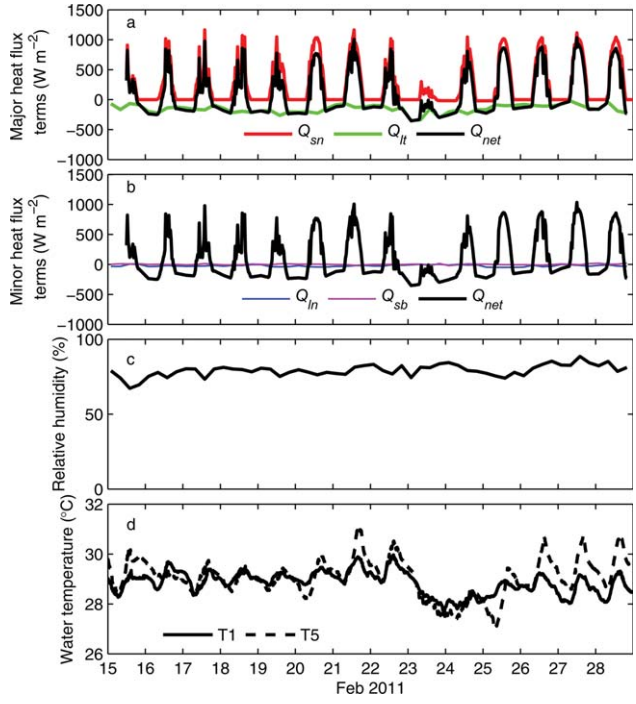

Figure 5. Atmospheric forcing conditions and SST responses between 15 February and 1 March 2011 at Coral Bay. (a) Major heat flux terms (net shortwave radiation $Q_{sn} = Q_{sd}(1 - \gamma_S)$ and latent heat flux Q_{lt}) from AIMS weather station and CFSRV2, (b) minor heat flux terms (net longwave radiation $Q_{ln} = Q_{ld} - Q_{lu}$ and sensible heat flux Q_{sb}) from CFSRV2, (c) relative humidity from CFSRV2, and (d) measured water temperatures at T1 and T5.

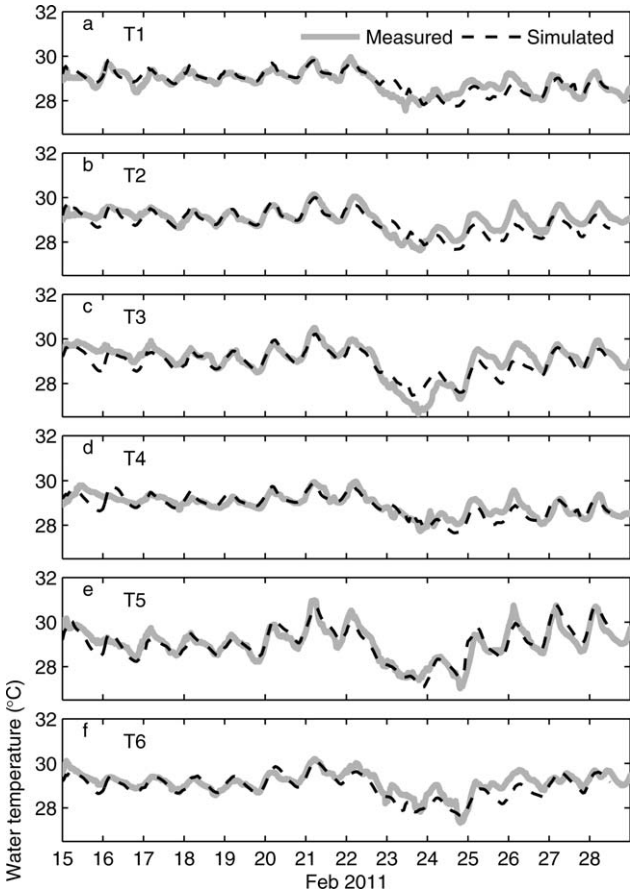

Figure 6. (a)–(f) Time series of the measured and simulated hourly water temperatures across Coral Bay (T1–T6).

humidity ranged between 65% and 90%, varying around a mean value of 80% (Figure 5c). The reflectance rates of shortwave radiation (total albedo) calculated based on water depth, habitat types, and tidal heights in Coral Bay were within the range of 0.08 to 0.20 for 90% of the reef domain with overall system average of 0.14 (see Appendix A).

[17] Mean daily water temperatures at the site near the reef crest closest to the ocean (T1) averaged around 29°C for the first 8 days, and then dropped to 28°C before slowly returning to around 28.5°C for the remaining 5 days (Figure 5d). Note that due to the wave-driven circulation patterns at this site [see *Zhang et al*., 2012], water is advected shoreward from the surf zone to T1 before entering the Coral Bay lagoon. The sudden decrease of temperature on 23rd Feb may be caused by the high cloud cover on that day but may also be due to the surface cooling caused by the deepening of the surface mixed layer as a result of increased offshore wind stresses from Tropical Cyclone Dianne moving off the coast of the North West Shelf of Western Australia around this time (15–22 February 2011). The amplitude of diurnal temperature variation (A_T defined as $\sqrt{2}$ times the standard deviation of the instantaneous temperatures over a 24 h period) at T1 averaged only ~0.3°C. Temperatures at the site furthest from the ocean (T5) also fluctuated around 29.2°C for the first 8 days but with a diurnal amplitude greater than at T1 (~0.5°C). Thus, maximum instantaneous temperatures at T5 reached over 30°C for 5 days (on 1st, 6–7th, and 13–14th Feb) over the 2 week period. The diurnal range at T5 was notably much greater for the last 3 days when the diurnal temperature amplitude at T5 reached ~0.8°C, more than double of that at T1 (~0.3°C). The mean daily temperature was also higher at T5 than at T1 (29.6°C versus 28.5°C) for each of these 3 days. Mean daily temperature and the diurnal amplitude of water temperature measured at all other locations fell within the ranges bound by T1 and T5.

3.2. Hindcast Simulations

[18] We found that the best fit between simulated and observed mean daily water temperature at T1 was achieved when we used an offshore SST of 29.2°C at the boundaries of the computational domain (Figure 1a) for the first 6 days, which linearly decreased to 27.2°C on the 7th day and then remained constant at 27.2°C for the rest of the hindcast period (6 days). This time-varying pattern of temperature agreed with the offshore SSTs observed by G1SST but differed in value by 1°C on average (consistent with the specified uncertainty for this SST product). The simulated water temperatures agreed well with the hourly measured water temperature at all locations for the 2 week simulation period (Figures 6 and 7), with correlations ranging between $r^2 = 0.57$ and 0.84 ($n = 326$) among locations and *rmse* and biases less than ~0.3°C each for all sites (Table 2). These results suggest little bias in the model given the reported absolute accuracy of the temperature loggers (±0.2°C). Furthermore, even though mean daily temperatures at T1 were used to adjust the mean daily offshore SST boundary condition (Figures 6a and 7a), the simulated diurnal variation in hourly water temperatures relative to mean daily temperature at T1 $\left(T(t) - \overline{T}_{24}\right)$ still showed reasonably good agreement with observed temperature residuals ($r^2 = 0.57$, $rmse = 0.21$°C, bias = 0.16°C, $n = 326$). Increasing the average total albedo from 0.09 to 0.23 only caused the daily net heat flux to decrease by less than 20 W m^{-2} and water temperatures to differ from the default simulation by only ±0.15°C on average across the domain. These results confirmed that improving the spatial characterization of total albedo (i.e., through maps of benthic habitat) would have marginally improved simulated water temperatures (Table 2). Decreasing the relative humidity (RH) to 50% (Hindcast 4) caused latent heat fluxes to decrease by 240 W m^{-2} on average and mean daily water temperature

Table 2. Hindcast Simulation Results[a]

	T1[b]	T2	T3	T4	T5	T6
r^2	0.57	0.64	0.76	0.70	0.84	0.76
rmse (°C)	0.21	0.32	0.38	0.28	0.31	0.26
bias (°C)	0.16	0.28	0.31	0.22	0.25	0.25
#2 – default (°C)	−0.06	−0.06	−0.09	−0.06	0.13	0.09
#3 – default (°C)	0.07	0.08	0.10	−0.07	−0.15	−0.10
#4 – default (°C)	−0.77	−0.86	−1.28	−0.82	−1.90	−1.21
#5 – default (°C)	0.39	0.44	0.66	0.41	0.99	0.62

[a]In default simulation, a spatial-averaged albedo of 0.14 and time-varying relative humidity (~80%) was applied. Hindcasts 2 and 3 tested the effect of albedo (0.08 and 0.20, respectively), whereas Hindcasts 4 and 5 tested the effect of relative humidity (50% and 95%, respectively).
[b]Reflects analysis of residual temperature (see text).

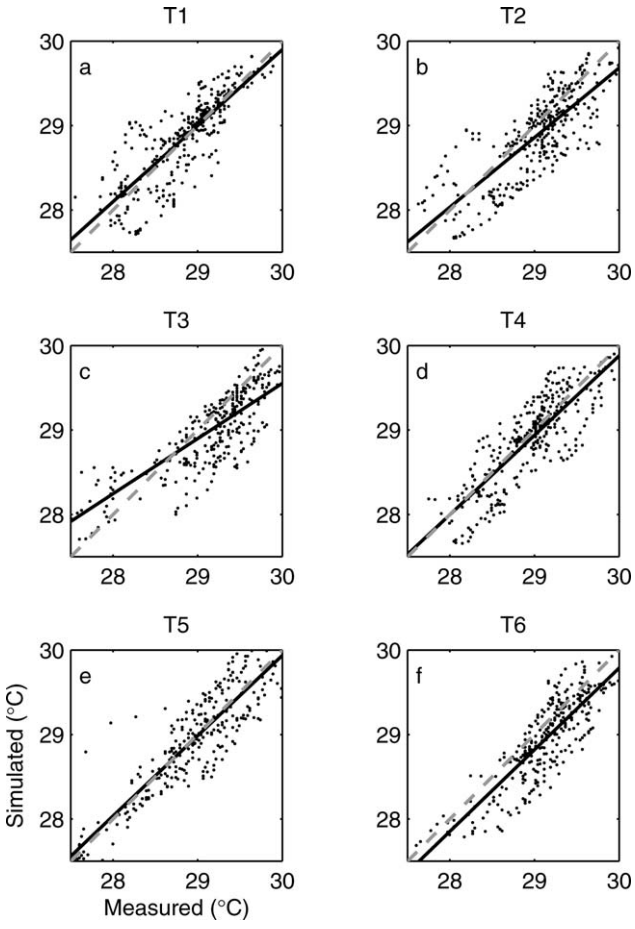

Figure 7. (a)–(f) Comparison between the simulated and measured water temperatures across Coral Bay (T1–T6). The black solid lines indicate regression lines and the grey dashed lines denote a 1:1 relationship.

to decrease by 0.7–2.0°C across Coral Bay (Table 2). In contrast, increasing RH from ~80% on average to 95% (Hindcast 5) caused daily average latent heat flux to increase on average by 120 W m^{-2} and mean daily water temperatures to increase by 0.4–1.0°C (Table 2).

3.3. Scenario Analysis Under Various Forcing Conditions

[19] To focus on the reef-scale variation in temperature due to the influence of local factors, we will direct most of our attention on the difference in mean daily temperature between the reef and offshore surface waters $(\overline{\Delta T})$ as well as the diurnal temperature variation amplitude (A_T) that was calculated based on the standard deviation σ_{24} of hourly temperature over a 24 h period $(A_T = \sqrt{2}\sigma_{24})$. Both $\overline{\Delta T}$ and A_T were then compared with the spatial distribution of residence time computed for this domain previously by *Zhang et al*. [2012]. For the default model case (Scenario 1), $\overline{\Delta T}$ increased with distance away from the reef flat (Figure 8a). This dependency of $\overline{\Delta T}$ on the reef location showed a strong linear dependency on local water residence times (Figures 8b and 9a); however, A_T exhibited a more complicated spatial pattern that could not be explained by residence time alone (Figure 9b). Note that the unexpectedly long residence times calculated near the exit of the South Channel (close to T4) was an artifact caused by the constant hydrodynamic forcing for the idealized simulations (see details in *Zhang et al*. [2012]).

[20] The simulated spatial patterns of $|\overline{\Delta T}|$ from all Scenario tests (1–13) and the spatial patterns of A_T from most Scenarios tests (1–7) were similar to those for default case and differed only in magnitude (Figure 10). Therefore, to simply compare our results across all scenarios, we first calculated the spatial averages of $|\overline{\Delta T}|$ and A_T across the Coral Bay domain (denoted as $\langle|\overline{\Delta T}|\rangle$ and $\langle A_T\rangle$), and next

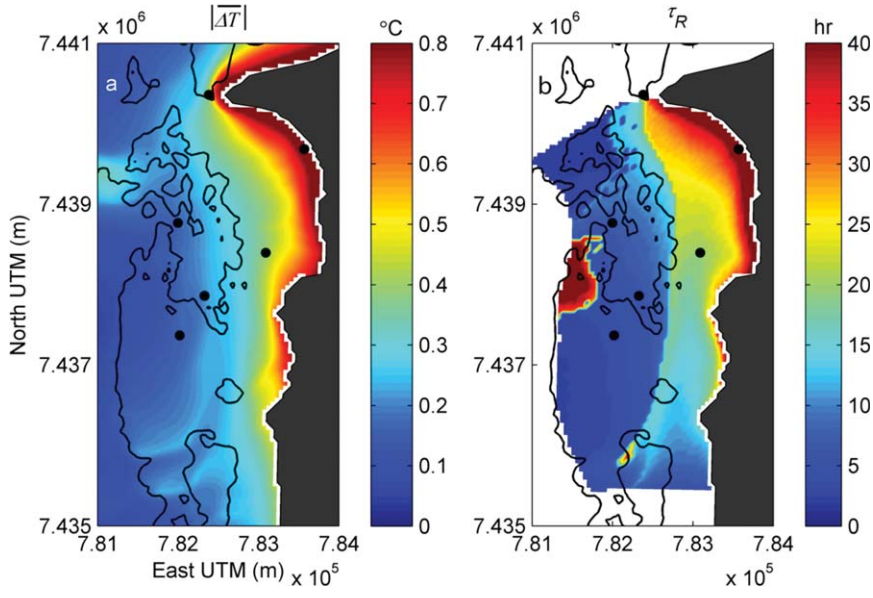

Figure 8. (a) Spatial map of daily-averaged temperature differences between reef waters and waters offshore ($|\overline{\Delta T}|$) for the default scenario test simulation (Scenario 1) and (b) Spatial map of residence times for Coral Bay under 2 m wave forcing condition from *Zhang et al*. [2012]. The black lines highlight the 4 m isobath.

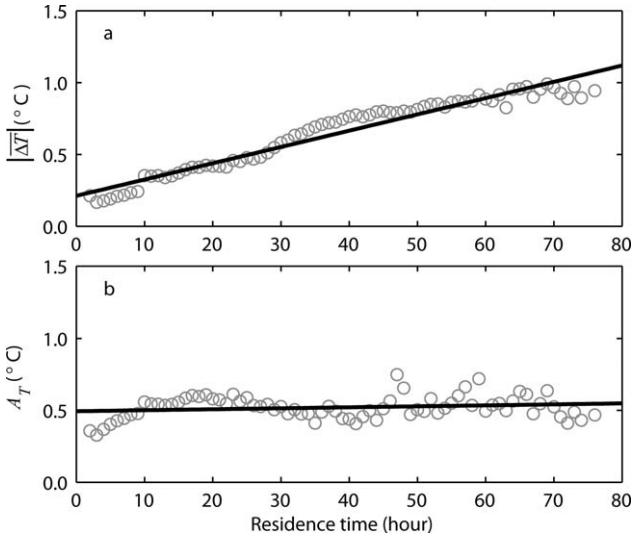

Figure 9. (a) Simulated differences between the mean daily reef and offshore water temperature ($|\overline{\Delta T}|$) and (b) simulated diurnal temperature amplitude (A_T) versus residence time (τ_R) calculated according to *Zhang et al*. [2012] for the default scenario test (Scenario 1). Only the bin-averaged $|\overline{\Delta T}|$ and A_T for the hourly residence time from 0 to 76 h are shown. The regression lines (in black) for the two datasets are for (a) $|\overline{\Delta T}| = 0.011\tau_R + 0.212$ ($r^2 = 0.94$, $n = 76$) and for (b) $A_T = 0.68 \times 10^{-3}\tau_R + 0.490$ ($r^2 = 0.03$, $n = 76$), respectively.

calculated the percentage of domain area where $|\overline{\Delta T}|$ or A_T was greater than temperature thresholds of 0.5°C and 1.0°C, respectively (Table 3). For the default model case (Scenario 1), $\langle|\overline{\Delta T}|\rangle$ was around 0.3°C while only 15% of the domain exhibited $|\overline{\Delta T}|$ greater than 0.5°C and less than 1% of the domain exhibited $|\overline{\Delta T}|$ greater than 1°C (Figure 10a). Only when $|\overline{Q_{net}}| \geq 150$ W m^{-2} (Scenarios 2 and 5) did $\geq 50\%$ of the domain exhibit $|\overline{\Delta T}| > 0.5$°C and $\geq 15\%$ of the domain exhibit $|\overline{\Delta T}| > 1$°C (Figure 10c). Overall, we found from the scenario simulations that $\langle|\overline{\Delta T}|\rangle$ was positively correlated with the daily net heat flux $|\overline{Q_{net}}|$ and inversely correlated with a "wave forcing factor" (F_w), defined as significant wave height times the square root of peak wave period ($F_w = H_S\sqrt{\tau_p}$), due to the inverse dependency of water residence times on wave-driven circulation [*Gourlay*, 1996; *Zhang et al*., 2012]. Thus, we found that a linear empirical relationship could be used to model $\langle|\overline{\Delta T}|\rangle$ as a function of $|\overline{Q_{net}}|/\left(H_S\sqrt{\tau_p}\right)$:

$$\langle|\overline{\Delta T}|\rangle = 0.02\left[|\overline{Q_{net}}|/\left(H_S\sqrt{\tau_p}\right)\right] + 0.04 \quad (5)$$

($r^2 = 0.97$, $p < 0.05$, $n = 10$; see Figure 11). Note that the correlations (r^2) between $|\overline{\Delta T}|$ and $|\overline{Q_{net}}|/\left(H_S\sqrt{\tau_p}\right)$ were greater than 0.75 for all grid cells within the Coral Bay domain ($p < 0.05$, $n = 10$).

[21] The average diurnal temperature amplitude $\langle A_T\rangle$ generally ranged between 0.3 and 0.6°C across all scenario simulations and demonstrated little clear dependency on $|\overline{Q_{net}}|$ or F_w; however, $\langle A_T\rangle$ was highly dependent on the magnitude of diurnal variation in $\overline{Q_{net}}$ (Table 3). A_T was generally greater than 0.5°C across 30–50% of the domain, except for the extreme values of diurnal $\overline{Q_{net}}$ amplitude, while only 4% or less of the domain exhibited A_T in excess of 1°C for all simulations (Scenarios 6 and 7; Table 3). Spatial patterns of A_T were nearly identical for scenarios where only the daily average or diurnal amplitude of the net daily heat flux was varied (Scenarios 1–7); however, they were still sensitive to H_s unlike for $|\overline{\Delta T}|$ (Scenarios 8–10; Figures 10 and 12). While areas with a local minimum value of $A_T \sim 0.3$°C could be observed at different locations in the inner lagoon for wave height conditions of 1 and 2 m, they were not observable for wave height conditions of 3 and 4 m (Figure 12). Finally, changing the direction of the alongshore current (Scenario 13) did not substantially change the magnitude or spatial pattern of either $|\overline{\Delta T}|$ or A_T across the entire domain (Table 3).

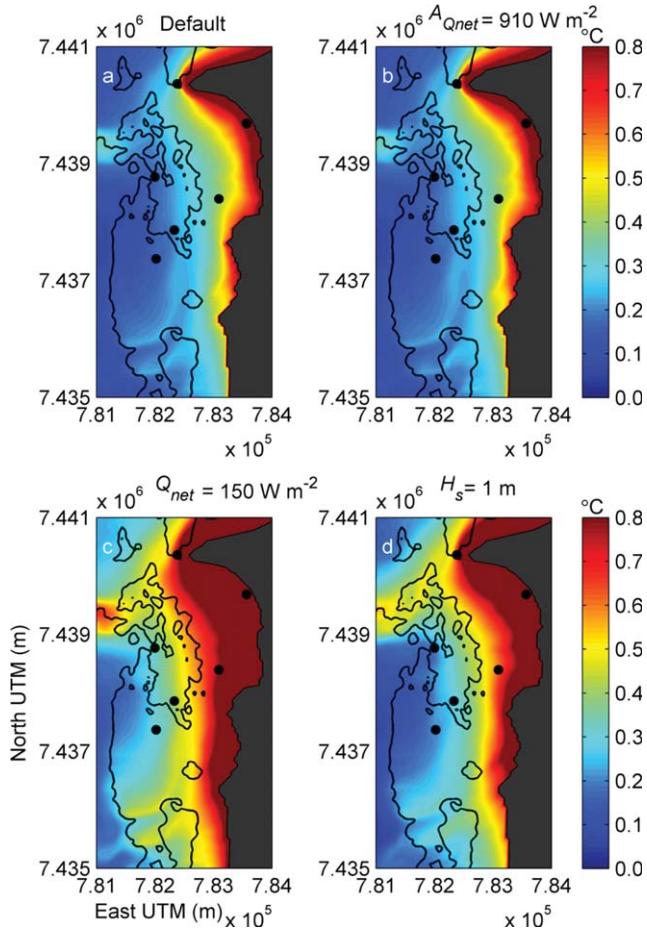

Figure 10. The spatial map of the differences between mean daily reef and offshore water temperature ($|\overline{\Delta T}|$) from select scenario test simulations where forcing variables are perturbed from their default values. (a) Scenario 1: default values, (b) Scenario 6: changing the diurnal amplitude of heat flux to 910 W m^{-2}, (c) Scenario 2: changing the mean daily net heat flux to 150 W m^{-2}, and (d) Scenario 8: changing the offshore wave height to 1 m.

Table 3. Scenario Tests Results[a]

Scenario	ΔT $\langle\lvert\overline{\Delta T}\rvert\rangle$ (°C)	ΔT $f_{>0.5}$ (%)	ΔT $f_{>1.0}$ (%)	A_T $\langle A_T\rangle$ (°C)	A_T $f_{>0.5}$ (%)	A_T $f_{>1.0}$ (%)
1 (default)	0.29	15	<1	0.41	30	<1
2 ($Q_{net}=150$)	0.57	50	15	0.42	40	<1
3 ($Q_{net}=0$)	0.03	0	0	0.42	37	<1
4 ($Q_{net}=-75$)	−0.26	12	0	0.41	30	<1
5 ($Q_{net}=-200$)	−0.69	67	24	0.41	35	<1
6($A_{Qnet}=910$)	0.28	15	<1	0.57	77	4
7($A_{Qnet}=390$)	0.32	18	0	0.27	3	0
8 ($H_S=1$)	0.44	35	7	0.45	42	1
9 ($H_S=3$)	0.21	8	0	0.44	47	1
10($H_S=4$)	0.15	2	0	0.40	27	<1
11($\tau_p=8$)	0.33	20	3	0.46	50	<1
12($\tau_p=16$)	0.30	15	<1	0.42	35	<1
13($U_{off}=$N)	0.28	15	<1	0.42	33	<1

[a]The default scenario was forced by a constant offshore significant wave height of 2 m, peak wave period of 12 s, southward alongshore current and a recurring diurnal heat flux with a daily average of +75 W m^{-2} and diurnal amplitude (max – min) of 650 W m^{-2}.

4. Discussion

[22] Our numerical model successfully reproduced the observed spatial and temporal variation in water temperature during the anomalously warm conditions that caused a mass bleaching event in Coral Bay (Figures 6 and 7). That the magnitude of the difference between mean daily temperatures within the reef and offshore increased as a function of residence time across the domain was consistent with the fact that water temperatures should increase with lengthened exposure to cumulative net heating (Figures 8 and 9a). Because water residence times in wave-driven systems such as Coral Bay are an inverse function of the square root of offshore incident wave energy flux [*Gourlay*, 1996; *Zhang et al*., 2012], which is proportional to the wave forcing factor (F_w), differences in daily mean water temperature between the reef and offshore were therefore correlated with the ratio of net surface heat flux to the wave forcing factor (Figure 11). In contrast, the amplitude of diurnal temperature variation appeared to increase with residence time during the first 10–20 h, but then decreased and became much more erratic on longer time scales (Figures 9b and 12). This is because when residence times become greater than half a day, temperature fluctuations may start to decrease due to the smoothing effect of integrating both positive and negative heating over longer portions of the diurnal heating cycle (see Figures 5a and 5b). That the spatial pattern of the diurnal amplitudes of temperature (A_T) varied with offshore wave forcing whereas the spatial mean of A_T remained similar for all six wave forcing scenarios emphasizes the complexity of the spatial structure of diurnal variations in water temperature in a real reef system (Figure 12 and Table 3); changes, which can only be resolved by a high-resolution coupled thermal-hydrodynamic model. Nonetheless, the spatially averaged A_T was linearly

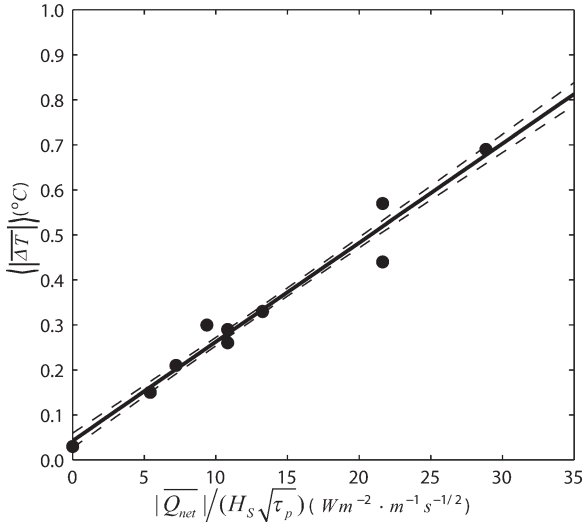

Figure 11. Coral Bay spatially averaged daily mean temperature relative to offshore $\langle|\overline{\Delta T}|\rangle$ as a function of daily net heat flux divided by wave forcing factor $\left(|\overline{Q_{net}}|/(H_S\sqrt{\tau_p})\right)$. The regression line is $\langle|\overline{\Delta T}|\rangle = 0.02\left[|\overline{Q_{net}}|/(H_S\sqrt{\tau_p})\right] + 0.04$ ($r^2 = 0.97$, $p < 0.05$, $n = 10$), as indicated by the solid black line. The 90% confidence levels for the regression are indicated by the black dashed lines.

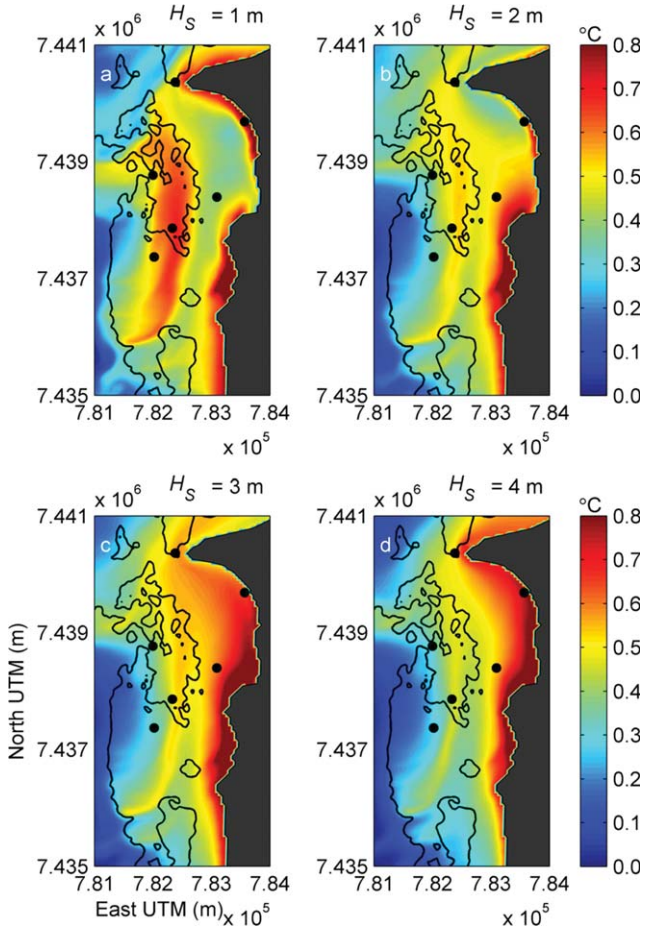

Figure 12. Spatial maps of the diurnal amplitude of temperature (A_T) from the scenario test simulations under various significant wave height conditions, which are 1 m (a: Scenario 8), 2 m (b: Scenario 1), 3 m (c: Scenario 9), and 4 m (d: Scenario 10).

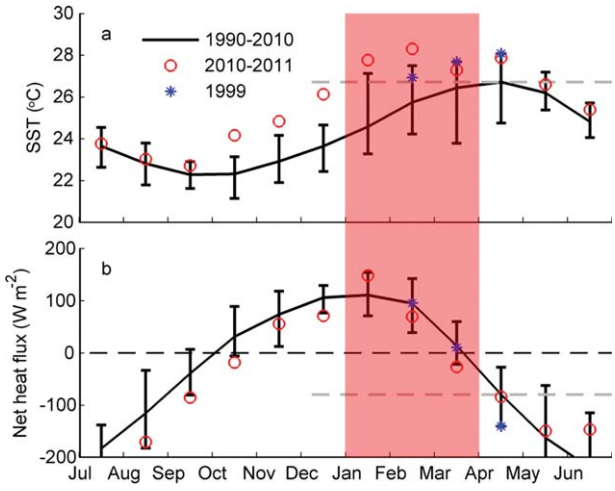

Figure 13. The monthly mean SST (a) and net heat flux (b) for 1990–2010 (black solid lines), 2010–2011 (red circles) and 1999 (blue stars). The error bars indicate the ranges of the historical data (1990–2010). The red mask highlights the summer months. The gray dashed lines indicate the monthly averaged SST (in Figure 13a) or the average daily net heat flux (in Figure 13b) during April when the maximum monthly mean in offshore SST normally occurs.

correlated with the diurnal amplitude of heat fluxes regardless of wave forcing (Table 3).

[23] Over the 3 month period of December 2010 through February 2011, SSTs offshore of Coral Bay reached values that were 2.7°C higher on average than their historical "normal" averages for this three-month period (Figure 13a). Scenario tests indicated that, under the average summer climatology for Coral Bay ($H_s = 2$ m and $\overline{Q_{\text{net}}} = 75$ W m^{-2}), the impact of local net heat fluxes on spatial reef water temperature anomalies was substantial for a relatively small fraction of the reef system; i.e., only 15% of the domain experienced differences in mean daily temperature that were greater than 0.5°C (Figure 10a and Table 3). Therefore, under typical summer conditions local net heating would normally have had only a marginal influence on local temperature anomalies. However, in the 5 week period from 1 January to 11 February when bleaching was recorded in Coral Bay [*Moore et al.*, 2012], daily net heat fluxes averaged 150 W m^{-2} (Figure 13b). This high level of net heat flux, together with the slightly lower wave heights (1.7 m on average), caused mean daily temperatures across Coral Bay to be 0.7°C higher than offshore on average and up to 1.5°C higher than offshore within the inner lagoon (Figure 14). These in situ observations along with our simulation results suggest that even though the elevated offshore temperatures were still the most significant source of anomalous warming within Coral Bay during the 2010–2011 marine heat wave [*Feng et al.*, 2013; *Pearce and Feng*, 2012], local heating nonetheless contributed significantly to temperature elevations inside the reef during the period leading up to the reported bleaching.

[24] One way to further investigate how much local heat fluxes exacerbated or ameliorated the thermal stress caused by the 2010–2011 marine heat wave would be to compare the number of degree heating weeks (DHW) that had accumulated both inside and outside the reef by the time bleaching had occurred [*Liu et al.*, 2003; *Strong et al.*, 2011] (coralreefwatch.noaa.gov/satellite/methodology/methodology). Briefly, DHW is defined as the integral of daily "HotSpots" greater than 1°C over a rolling twelve-week period, where HotSpot is the difference between the mean daily temperature and the maximum monthly mean (MMM) as derived from the historical climatology for a given reef site [*Glynn and Dcroz*, 1990; *Liu et al.*, 2003, 2005]. A time series of offshore HotSpots was first calculated from the 1 km blended global SST data using a historical temperature climatology calculated from the longer 25 km blended SST data record (see Figures 15a and 15b). To calculate DHW for sites within the Coral Bay domain, we first used linear relationships between $\overline{\Delta T}$ and $\overline{Q}_{\text{net}}/H_S\sqrt{\tau_p}$ for each grid cell (similar to that shown in Figure 11) derived from a wide range of wave and atmospheric forcings covered by the Scenario simulations to generate temporally and spatially dependent maps of differences in mean daily temperature ($\overline{\Delta T}$) across the Coral Bay domain over a 1 year period of time (from October 2010 to September 2011). We then generated time series of in situ temperatures for each grid cell over a twelve-month period by adding these spatial maps of $\overline{\Delta T}$ to the offshore daily SST time series (1 km blended).

[25] Our calculations indicate that temperatures across Coral Bay were on average 0.5°C higher than offshore between November 2010 and February 2011 and 0.7°C higher between 1 January and mid-February 2011 due to the higher net heat fluxes during this period (Figure 15a).

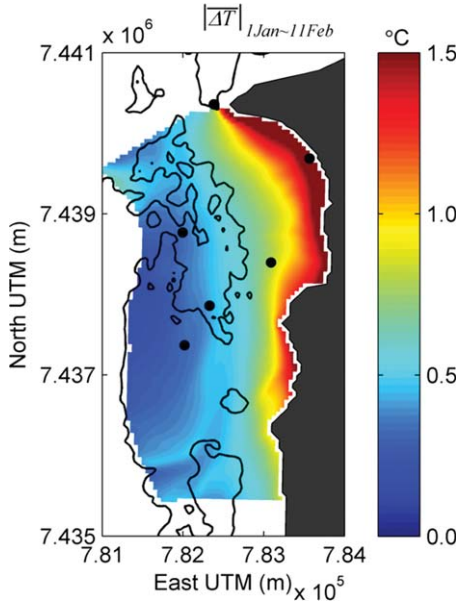

Figure 14. Map of the difference between the average daily temperature of reef waters and waters offshore $|\overline{\Delta T}|$ averaged over the period from 1 January 2010 to 11 February 2011. This map was derived from the spatial map of $|\overline{\Delta T}|$ for the default scenario, the linear relationship between $|\overline{\Delta T}|$ and $|\overline{Q_{net}}|/\left(H_S\sqrt{\tau_p}\right)$ as in Figure 11, and the net heat flux and wave condition over the period from 1 January to 11 February 2011. The black lines highlight the 4 m isobath.

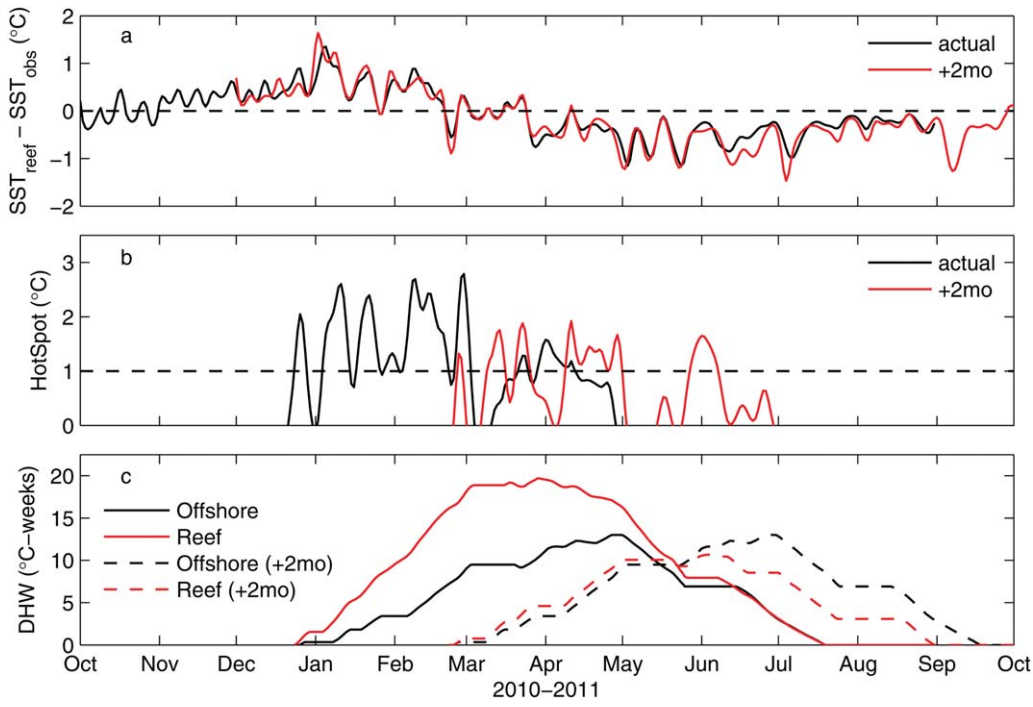

Figure 15. (a) The difference between spatially averaged reef SSTs and the observed offshore SST (G1SST), (b) reef Hotspots calculated from the spatially averaged reef SSTs, and (c) average DHWs for the entire Coral Bay reef domain and for offshore around the mass bleaching event in 2010–-2011. The legend label "+2mo" indicates a hypothetical scenario in which the marine heat wave had arrived 2 months later than the actual event.

HotSpots calculated based on the actual reef water temperatures rather than offshore water temperatures showed that the average temperature anomalies for the entire Coral Bay domain exceeded 1°C from early January to end of February (Figure 15b). Thus, the resulting average DHW calculated for the entire reef domain reached a maximum of 19°C-weeks by the end of February; a value more than twice as high as that reached by the offshore DHW over the same period (9°C-weeks, Figure 15c). Our simulations further show that the DHW first reached critical levels (8°C-weeks) along the landward side of the lagoon and then moved seaward across the lagoon and reef flat (Figure 16, and the auxiliary information for further description). The reason for this disparity in the timing and magnitude of DHW inside Coral Bay versus offshore is a direct result of the timing of the 2010–2011 marine heat wave that began in October 2010. When offshore temperatures associated with this heat wave peaked in late January to early February, net daily heat fluxes at Coral Bay were averaging 150 W m^{-2} (Figure 13a). This contrasts with more "typical" years when maximum reef water temperatures peak in late March to mid-April and daily net heat fluxes average −50 W m^{-2} due to seasonally increasing wind speeds and seasonally decreasing air temperatures (Figure 13b). Thus, the early arrival of the marine heat wave combined with higher than average summer atmospheric heat fluxes was equivalent to a ∼200 W m^{-2} increase in the net thermal forcing during peak seasonal offshore temperatures in comparison with more "normal" years. Our simulations indicate that under typical wave forcing, an increase in the net heat flux of this magnitude is big enough to increase $\overline{\Delta T}$ across Coral Bay by ∼0.8°C on average and more than 1.0°C for at least 20% of reef domain area. Furthermore, because the temperature of reef waters were already near or above their threshold for thermal stress as a result of the regional ocean warming (i.e., $T >$ maximum monthly mean +1°C or $T > 27.7$°C), any additional increases in reef water temperature of around ∼1°C or more due to seasonally elevated atmospheric thermal forcing would have greatly exacerbated existing levels of thermal stress brought on by the regional ocean warming. These results can help explain why the mass bleaching in Coral Bay was observed to have occurred by early February when the average reef DHW had already reached 11°C-weeks [*Moore et al*., 2012] even though offshore DHW was still just 3°C-weeks by this time and, therefore, below the threshold for even minor bleaching (4°C-weeks) [*Eakin et al*., 2009; *Liu et al*., 2005; *Strong et al*., 2011] (Figure 15c).

[26] To further illustrate how the timing of the marine heat wave influenced reef-scale thermal stresses, we can simulate what the effect of the 2010–2011 marine heat wave would have been if it had arrived 2 months later and in phase with the normal seasonal peak in offshore water temperatures. In such a hypothetical scenario, the timing and magnitude of the DHW for the reef-lagoon system at Coral Bay would not have been that different from offshore (Figure 15c). In fact, the maximum average DHW reached by the reef would have been less than that reached offshore (10 versus 13°C-weeks), albeit still beyond the threshold for critical bleaching. Although the spatial trend of DHW increasing seaward from the inner lagoon in this hypothetical scenario would have been similar to that of the real heat

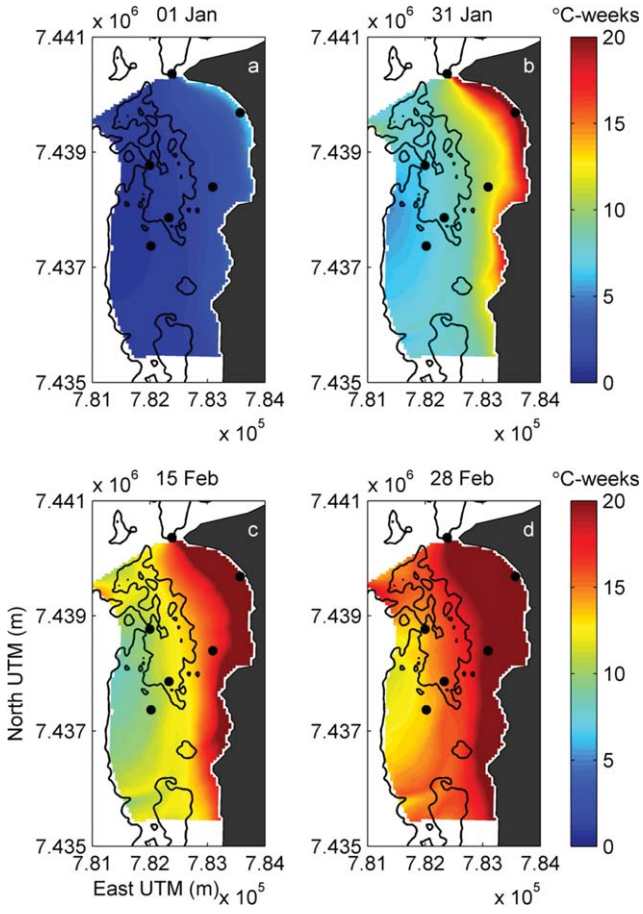

Figure 16. Maps of degree heating weeks accumulated on (a) 1 January, (b) 31 January, (c) 15 February, and (d) 28 February 2011 within Coral Bay domain. To better illustrate changes in the spatial pattern of DHWs, all values greater than or equal to 20°C-weeks are shown as having the same color. Mass bleaching within Coral Bay was reported by *Moore et al*. [2012] by 11 February.

wave, the magnitude of these changes would clearly have been different (see the auxiliary information for further description). Another way to demonstrate the importance of timing of these events is to compare the 2010–2011 heat wave against another historic heat wave in 1999 when offshore temperatures also reached maximum values in excess of 28°C, but during the normal peak seasonal temperature period in April (Figure 13a). The mean net daily heat fluxes in March and April of 1999 averaged -65 W m^{-2} or slightly lower than their historical average of -45 W m^{-2} for this same period (Figure 13b). This contrasts with the $+150$ W m^{-2} of extra net thermal forcing experienced by Coral Bay during the period leading up to the observed bleaching in February 2011. Under these conditions, we calculate that the DHW inside Coral Bay likely reached a maximum of just 8°C-weeks on average by late April 1999. It is therefore not surprising that there were no similar accounts of mass coral bleaching reported in Coral Bay or other parts of Ningaloo during the 1999 event even if offshore temperatures reached levels comparable to those observed in the summer of 2010–2011. The fact that no coral bleaching was observed at Coral Bay during this thermal event even when DHWs inside the reef were beyond the bleaching threshold could be due to a combination of greater resiliency of corals exposed to naturally greater temperature variation [*Carilli et al*., 2012; *Castillo et al*., 2012] and reduced light stress in April as compared with January [*Fabricius*, 2006; *Lesser*, 1997].

[27] Our results are particularly important given that at present there are no known records of thermal-induced mass bleaching across Ningaloo prior to the recent marine heat wave. If this phenomenon is indicative of a more persistent shift in climate dynamics across the Indo-Pacific region, then Ningaloo may further experience such marine heat waves under atmospheric conditions that will continue to exacerbate existing levels of thermal stress brought on by regional ocean warming. Our results further suggest much of the perceived ability (or inability) of current temperature-driven bleaching indices to predict inshore bleaching events from offshore SST data may stem from differences between inshore and offshore temperature dynamics and climatologies [*Maynard et al*., 2008; *McClanahan et al*., 2007; *Weeks et al*., 2008]. The numerical model framework we present here provides us with the means to reconstruct more accurate inshore reef water temperature climatologies thermal stress indices from longer term records of offshore SST, offshore wave forcing, and net atmospheric heat fluxes based on fundamental principles of oceanic and atmospheric physics.

[28] Our study focused on modeling reef-scale variations in seawater temperature driven by local atmospheric and wave forcing. The changes in offshore water temperature adjacent to the reef system were not resolved by our numerical model but instead assimilated from a temperature logger on the reef flat site (T1). We made this simplification, since to properly model the water temperature offshore of Coral Bay would require resolving large-scale hydrodynamic and thermodynamic processes off Ningaloo Shelf, such as coastal upwelling, vertical mixing or stratification, regional wind and heat fluxes, and transport by coastal current, eddies, and nonlinear internal waves [*Castillo and Lima*, 2010; *Glynn and Dcroz*, 1990; *Leichter et al*., 2006; *Monismith et al*., 2006; *Riegl and Piller*, 2003; *Wells et al*., 2012]. All these factors are known to cause the spatial and temporal variations in nearshore temperature profiles and are thus relevant factors for thermal bleaching events within coral reef systems. Although this study does not fully explore the effects of all these relevant bleaching factors, it is the first step to apply and validate such a numerical approach to mechanistically model the processes driving changes in water temperature within a reef system. In future studies, a nested model that links the processes and oceanic variables between a reef system (e.g., our study) and the continental shelf [e.g., *Xu et al*., 2013] can potentially be a promising tool to predict reef water temperature driven by hydrodynamic and atmospheric processes both nearshore and offshore.

5. Conclusions

[29] This study demonstrates the ability of numerical models to resolve the high-resolution spatial and temporal variation in water temperature across an entire reef system using a combination of oceanic and atmospheric forcing

provided by global wave and climate models (e.g., WaveWatch III and CFSRV2). Our results show that in Coral Bay, local heating and wave forcing can affect the spatial and temporal variation in water temperatures across an entire reef system. The impact of local heating is substantial in the inner lagoon under normal weather conditions and over the entire reef domain under more extreme weather conditions (e.g., high light, high humidity, low winds, and low waves). Nonetheless, local heat budgets can exacerbate the thermal stress caused by regional ocean warming, especially if the timing of such events occurs when net atmospheric heat fluxes are seasonally maximal or otherwise abnormally high. We show that an approach based on realistic estimation of atmospheric heating and circulation together with an incorporation of offshore boundary conditions can provide accurate and realistic simulations of local temperature anomalies and thermal stress. We believe that the present modeling approach can provide a means to more reliably and accurately predict the timing and magnitude of future bleaching events within reef systems due to global warming, especially when nested within a regional or global hydrodynamic-thermodynamic model. It further provides a valuable tool for downscaling regionally modeled climate variables and differentiating the roles of local versus global factors on the dynamics of coral reef systems [*Donner et al*., 2009; *Obura*, 2005]. The spatial pattern of reef water temperature resolved by our model during the bleaching period is especially informative given that this was the first thermal-induced mass bleaching ever recorded along Ningaloo Reef.

Appendix A: Calculating Total Albedo at Coral Bay

[30] The following calculation of the total albedo is based on *Kirk* [2011]. When incident light reaches the water surface, a fraction of the shortwave radiation is reflected back into the air and the rest penetrates the air-sea interface. The reflected flux (denoted as $L_{us}(0^+)$) and the surface-penetrating flux (denoted as $E_d(0^-)$) can be parameterized by

$$L_{us}(0^+) = E_d(0^+)\overline{\rho} \tag{A1}$$

$$E_d(0^-) \approx E_d(0^+)(1-\overline{\rho}) \tag{A2}$$

where 0^+ or 0^- denotes radiation just above or below the water surface ($z=0$) and $\overline{\rho}$ is the surface reflectance at the air-water interface. The upward scattering of shortwave radiation can usually be ignored in ocean waters and is thus not considered in equation (A2).

[31] The downward shortwave radiation in the water column (denoted as $E_d(z)$) attenuates with depth (z). If we assume that the reflection by particles in the water is negligible, shortwave radiation reaching the bottom can be described as

$$E_d(h) = E_d(0^-)e^{-k_d \cdot h} \tag{A3}$$

where h is the water depth.

[32] A fraction of the radiation reaching the bottom gets absorbed by the benthos and the rest of it is reflected upward as

$$L_u(h) = E_d(h) \cdot \gamma_b \tag{A4}$$

where γ_b is the bottom reflectance.

[33] This bottom-reflected flux again attenuates as it travels upward within the water column and the remaining flux reaching the water surface can be calculated by

$$L_u(0^-) = L_u(h)e^{-k_d \cdot h} \tag{A5}$$

[34] At the water surface, a fraction of the upward radiation is reflected back into the water column, and the rest of

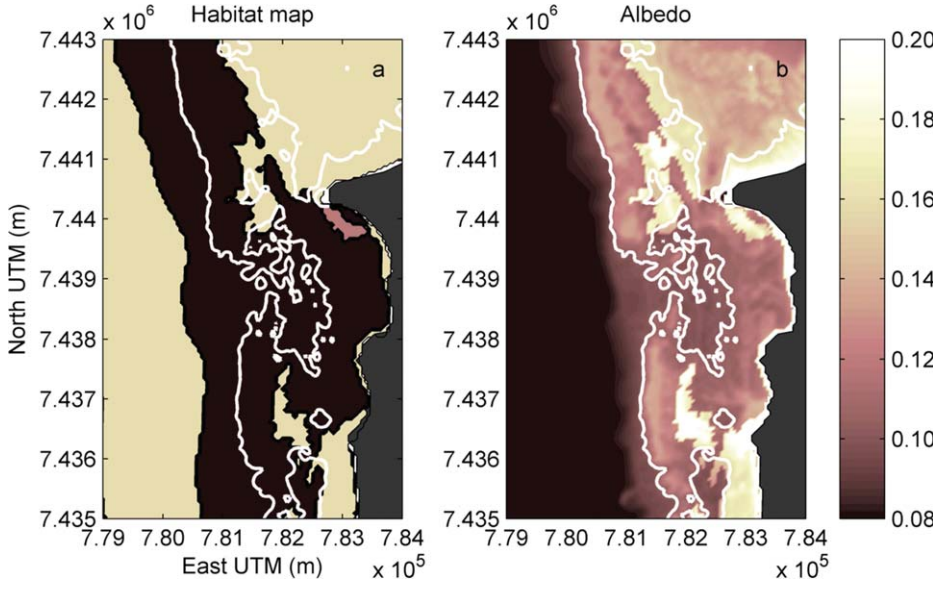

Figure A1. Close-up view of (a) a benthic habitat map and (b) a spatial map of albedo (benthos plus water column) for Coral Bay when the tidal elevation is zero (i.e., at mean sea level). In Figure A1a, the areas colored by yellow, dark red, and pink represent benthic types of sandy, coral reef, and colonized rubble, respectively. The white contour lines in both maps indicate the 4 m isobath.

it crosses the air-sea interface by refraction, which can be described as

$$L_{ur}(0^+) \approx 0.544 L_u(0^-) \tag{A6}$$

where the factor 0.544 is an empirical coefficient for relating radiance just above the surface to the corresponding radiance just below the surface.

[35] The total albedo (γ_S) is equal to the ratio of total upward shortwave radiation ($L_u(0^+)$) versus the incident downward shortwave radiation ($E_d(0^+)$) at the water surface. The total upward shortwave radiation includes the reflected radiation at the water surface $L_{us}(0^+)$ (calculated by equation (A(1))) and the residual upward radiation leaving the water surface $L_{ur}(0^+)$ (calculated by equations (A1)–(A6)). From equations (A1)–(A6), we obtain

$$\gamma_S = \frac{L_u(0^+)}{E_d(0^+)} \approx \underbrace{\overline{\rho}}_{surface} + \underbrace{(1-\overline{\rho}) \cdot 0.544 e^{-2k_d \cdot h} \gamma_b}_{bottom} \tag{A7}$$

where the first term on the right hand side of the equation represents the surface albedo and the second term represents the bottom albedo.

[36] The reflected light of $L_{ur}(0^-)$ at the water-air interface will reenter the water column, get attenuated, and be reflected upward again at the bottom, but only less than 10% of this reflected light will eventually leave the water surface. Therefore, we only consider the first-order term γ_S as the total albedo in shallow water.

[37] The surface reflectance $\overline{\rho}$ at Coral Bay is equal to 4% according to the ratio of upward and downward shortwave radiation at the water surface provided by NCEP CFSRV2 data for an offshore region adjacent to the study site; in this deep-ocean region where bottom albedo can be ignored, total albedo is approximately equal to surface albedo, i.e., $\overline{\rho} \approx L_u(0^+)/E_d(0^+)$. We used 0.14 for the light extinction coefficient (k_d), which was the measured coefficient for this study site during a previous experiment [*Zhang et al.*, 2012]. The bottom reflectance (γ_b) was decided by benthic type. According to the benthic habitat map (provided by Dept. of Environment and Conservation, Western Australia) and a high-resolution aerial photograph within the study area (with spatial resolution ranging from 20 to 100 m), the benthic types were classified as coral reef, sand, and colonized rubble (see Figure A1a) and the bottom reflectance for the three benthic types are 0.14, 0.46, and 0.32, respectively [*Hochberg et al.*, 2003]. The total albedo can thus be calculated as a function of depth and benthic reflectance (equation (A3)). The total albedo for Coral Bay is within the range of 0.14 ± 0.06, which covers 90% of the spatial area within the shallow water ($h \leq 10$ m) when tidal heights varied within the range of ± 0.6 m (see Figure A1b).

Notation

Variable	Description
A_{Qnet}	diurnal amplitude of net air-sea heat fluxes, W m^{-2}.
A_T	diurnal temperature variation amplitude, °C.
$\langle A_T \rangle$	spatial mean of A_T across the Coral Bay domain, °C.
C_H	heat exchange coefficient for sensible heat.
C_p	specific heat of air at constant pressure, J kg^{-1} °C^{-1}.
C_w	heat exchange coefficient for latent heat.
dir	wave direction rotating clockwise from the North, °.
F_w	wave forcing factor which is proportional to the square root of offshore wave energy flux, m $s^{-1/2}$.
h	water depth, m.
H_S	incoming significant wave height from offshore, m.
L_v	latent heat of vaporization, J kg^{-1}.
q_{10}	specific humidity at 10 m above the water surface, kg kg^{-1}.
q_s	saturated specific humidity at the water surface, kg kg^{-1}.
Q_{ld}	downward longwave radiation, W m^{-2}.
Q_{ln}	net longwave radiation, W m^{-2}.
Q_{lt}	latent heat flux, W m^{-2}.
Q_{lu}	upward longwave radiation, W m^{-2}.
$\overline{Q_{net}}$	daily mean of Q_{net}, W m^{-2}.
Q_{net}	net air-sea heat fluxes, W m^{-2}.
Q_{sb}	sensible heat flux, W m^{-2}.
Q_{sd}	downward shortwave radiation, W m^{-2}.
Q_{sn}	net shortwave radiation, W m^{-2}.
r^2	R square.
$rmse$	root-mean-square error.
RH	relative humidity.
T	reef water temperature, °C.
T_{air}	air temperature at 10 m above the water surface, °C.
T_s	water surface temperature, °C.
U_{10}	wind speed at 10 m above the water surface, m s^{-1}.
γ_S	total albedo.
ΔT	Temperature difference between reef and offshore surface waters, °C.
$\overline{\Delta T}$	daily mean of ΔT, °C.
$\langle \lvert\overline{\Delta T}\rvert \rangle$	spatial mean of $\lvert\overline{\Delta T}\rvert$ across the Coral Bay domain, °C.
ρ_{air}	air density, kg m^{-3}.
ρ_w	water density, kg m^{-3}.
σ_{24}	standard deviation of the hourly reef water temperature over a day, °C.
τ_p	peak wave period, s.
τ_R	residence time, hour.

[38] **Acknowledgments.** This work was supported by iVEC through the use of supercomputing resources provided through The Australian Resources Research Centre (ARRC). Funding was provided by an Australian Research Council Super Science Fellowship FS110200021 to Z.Z. and Future Fellowship FT110100201 to R.L. M.Mc., J.F., and Z.Z. gratefully acknowledge the invaluable support provided by the ARC Centre of excellence in Coral Reef studies and to Frazer McGregor for help in collecting the temperature data. The authors also appreciate the maintenance and supply of CFSRV2 global atmospheric reanalysis data from the Research Data Archive (RDA) by the Computational and Information Systems Laboratory (CISL) at the National Center for Atmospheric Research (NCAR) and the operational global wave model WaveWatch III output by NOAA/National Weather Service.

References

Berkelmans, R. (2009), Bleaching and mortality thresholds: How much is too much?, in *Coral Bleaching: Patterns, Processes, Causes and*

Consequences, edited by M. J. H. van Oppen and J. M. Lough, pp. 103–119, Springer, Berlin.

Berkelmans, R., G. De'ath, S. Kininmonth, and W. J. Skirving (2004), A comparison of the 1998 and 2002 coral bleaching events on the Great Barrier Reef: Spatial correlation, patterns, and predictions, *Coral Reefs*, *23*(1), 74–83, doi:10.1007/S00338-003-0353-Y.

Booij, N., R. C. Ris, and L. H. Holthuijsen (1999), A third-generation wave model for coastal regions: 1. Model description and validation, *J. Geophys. Res.*, *104*(C4), 7649–7666.

Carilli, J., S. D. Donner, and A. C. Hartmann (2012), Historical temperature variability affects coral response to heat stress, *Plos One*, *7*(3), e34418, doi: 10.1371/JOURNAL.PONE.0034418.

Cassata, L., and L. B. Collins (2008), Coral reef communities, habitats, and substrates in and near sanctuary zones of Ningaloo Marine Park, *J. Coastal Res.*, *24*(1), 139–151, doi:10.2112/05–0623.1.

Castillo, K. D., and F. P. Lima (2010), Comparison of in situ and satellite-derived (MODIS-Aqua/Terra) methods for assessing temperatures on coral reefs, *Limnol. Oceanogr. Methods*, *8*, 107–117.

Castillo, K. D., J. B. Ries, J. M. Weiss, and F. P. Lima (2012), Decline of forereef corals in response to recent warming linked to history of thermal exposure, *Nat. Clim. Change*, *2*(10), 756–760.

Chao, Y., Z. J. Li, J. D. Farrara, and P. Hung (2009), Blending sea surface temperatures from multiple satellites and in situ observations for coastal oceans, *J. Atmos. Oceanic Technol.*, *26*(7), 1415–1426, doi:10.1175/2009JTECHO592.1.

Cook, C. B., A. Logan, J. Ward, B. Luckhurst, and C. J. Berg (1990), Elevated temperatures and bleaching on a high latitude coral reef: The 1988 Bermuda Event, *Coral Reefs*, *9*(1), 45–49, doi:10.1007/BF00686721.

Coronado, C., J. Candela, R. Iglesias-Prieto, J. Sheinbaum, M. Lopez, and F. J. Ocampo-Torres (2007), On the circulation in the Puerto Morelos fringing reef lagoon, *Coral Reefs*, *26*(1), 149–163, doi:10.1007/S00338-006-0175-9.

Davis, K. A., S. J. Lentz, J. Pineda, J. T. Farrar, V. R. Starczak, and J. H. Churchill (2011), Observations of the thermal environment on Red Sea platform reefs: A heat budget analysis, *Coral Reefs*, *30*, 25–36, doi:10.1007/S00338-011-0740-8.

Depczynski, M., et al. (2013), Bleaching, coral mortality and subsequent survivorship on a West Australian fringing reef, *Coral Reefs*, *32*(1), 233–238.

Donner, S. D., T. R. Knutson, and M. Oppenheimer (2007), Model-based assessment of the role of human-induced climate change in the 2005 Caribbean coral bleaching event, *Proc. Natl. Acad. Sci. U. S. A.*, *104*(13), 5483–5488, doi:10.1073/PNAS.0610122104.

Donner, S. D., S. F. Heron, and W. J. Skirving (2009), Future scenarios: A review of modelling efforts to predict the future of coral reefs in an era of climate change, in *Coral Bleaching: Patterns, Processes, Causes and Consequences*, edited by M. J. H. van Oppen and J. M. Lough, pp. 159–173, Springer, Berlin.

Eakin, C. M., J. M. Lough, and S. F. Heron (2009), Climate variability and change: Monitoring data and evidence for increased coral bleaching stress, in *Coral Bleaching: Patterns, Processes, Causes and Consequences*, edited by M. J. H. van Oppen and J. M. Lough, pp. 41–67, Springer, Berlin.

Egbert, G. D., A. F. Bennett, and M. G. G. Foreman (1994), Topex/poseidon tides estimated using a global inverse model, *J. Geophys. Res.*, *99*, 24,821–24,852.

Eidenshink, J. C., and J. L. Faundeen (1994), The 1 km AVHRR global land data set: First stages in implementation, *Int. J. Remote Sens.*, *15*(17), 3443–3462, doi:10.1080/01431169408954339.

Fabricius, K. E. (2006), Effects of irradiance, flow, and colony pigmentation on the temperature microenvironment around corals: Implications for coral bleaching?, *Limnol. Oceanogr.*, *51*(1), 30–37.

Fairall, C. W., E. F. Bradley, J. E. Hare, A. A. Grachev, and J. B. Edson (2003), Bulk parameterization of air-sea fluxes: Updates and verification for the COARE algorithm, *J. Clim.*, *16*(4), 571–591, doi:10.1175/1520-0442(2003)016<0571:BPOASF>2.0.CO;2.

Falter, J. L., R. J. Lowe, Z. Zhang, and M. McCulloch (2013), Physical and biological controls on the carbonate chemistry of coral reef waters: Effects of metabolism, *wave forcing, sea level, and geomorphology, Plos One*, *8*(1), e53303, doi:10.1371/JOURNAL.PONE.0053303.

Feng, M., M. J. McPhaden, S. P. Xie, and J. Hafner (2013), La Niña forces unprecedented Leeuwin Current warming in 2011, *Nat. Sci. Rep.*, *3*, 1277, doi:10.1038/SREP01277.

Franklin, G., I. Mariño-Tapia, and A. Torres-Freyermuth (2013), Effects of reef roughness on wave setup and surf zone currents, in *Proceedings 12th International Coastal Symposium*, edited by D. C. Conley, G. Masselink, P. E. Russell and T. J. O'Hare, pp. 2005–2010, Journal of Coastal Research, Special Issue No. 65, Plymouth, England.

Frieler, K., M. Meinshausen, A. Golly, M. Mengel, K. Lebek, S. D. Donner, and O. Hoegh-Guldberg (2010), Limiting global warming to 2°C is unlikely to save most coral reefs, *Nat. Clim. Change*, 3, 165–170, doi:10.1038/NCLIMATE1674.

Geernaert, G. L., S. E. Larsen, and F. Hansen (1987), Measurements of the wind stress, heat flux, and turbulence intensity during storm conditions over the North Sea, *J. Geophys. Res.*, *92*, 13,127–13,139.

Gill, J. A., A. R. Watkinson, J. P. McWilliams, and I. M. Cote (2006), Opposing forces of aerosol cooling and El Niño drive coral bleaching on Caribbean reefs, *Proc. Natl. Acad. Sci. U. S. A.*, *103*(49), 18,870–18,873, doi:10.1073/PNAS.0608470103.

Glynn, P. W. (1993), Coral reef bleaching: Ecological perspectives, *Coral Reefs*, *12*(1), 1–17.

Glynn, P. W., and L. Dcroz (1990), Experimental evidence for high temperature stress as the cause of El Niño-coincident coral mortality, *Coral Reefs*, *8*(4), 181–191.

Gourlay, M. R. (1996), Wave set-up on coral reefs: 1. Set-up and wave-generated flow on an idealised two dimensional horizontal reef, *Coastal Eng.*, *27*, 161–193.

Heron, S. F., R. L. Pressey, W. J. Skirving, J. L. Rauenzahn, B. A. Parker, and C. M. Eakin (2012), Identifying oceanic thermal anomalies in the coral triangle region, paper presented at the 12th International Coral Reef Symposium, Cairns, Qld., Australia.

Hochberg, E. J., M. J. Atkinson, and S. Andrefouet (2003), Spectral reflectance of coral reef bottom-types worldwide and implications for coral reef remote sensing, *Remote Sens. Environ.*, *85*(2), 159–173.

Hoegh-Guldberg, O. (1999), Climate change, coral bleaching and the future of the world's coral reefs, *Mar. Freshwater Res.*, *50*(8), 839–866.

Hoegh-Guldberg, O., and B. Salvat (1995), Periodic mass-bleaching and elevated sea temperatures: Bleaching of outer reef slope communities in Moorea, French Polynesia, *Mar. Ecol. Prog. Ser.*, *121*(1-3), 181–190.

Ivey, G., and J. C. Patterson (1984), A model of the vertical mixing in Lake Erie in summer, *Limnol. Oceanogr.*, *29*(3), 553–563.

Jokiel, P. L., and E. K. Brown (2004), Global warming, regional trends and inshore environmental conditions influence coral bleaching in Hawaii, *Global Change Biol.*, *10*(10), 1627–1641.

Kirk, J. T. O. (2011), Light and Photosynthesis in Aquatic Ecosystems, 3rd ed., Cambridge Univ. Press, Cambridge.

Kumar, N., G. Voulgaris, J. C. Warner, and M. Olabarrieta (2012), Implementation of the vortex force formalism in the coupled ocean-atmosphere-wave-sediment transport (COAWST) modeling system for inner shelf and surf zone applications, *Ocean Modell.*, *47*, 65–95, doi:10.1016/J.OCEMOD.2012.01.003.

Leichter, J. J., B. Helmuth, and A. M. Fischer (2006), Variation beneath the surface: quantifying complex thermal environments on coral reefs in the Caribbean, Bahamas and Florida, *J. Mar. Res.*, *64*(4), 563–588, doi:10.1357/002224006778715711.

Lenihan, H. S., M. Adjeroud, M. J. Kotchen, J. L. Hench, and T. Nakamura (2008), Reef structure regulates small-scale spatial variation in coral bleaching, *Mar. Ecol. Prog. Ser.*, *370*, 127–141, doi:10.3354/MEPS07622.

Lesser, M. P. (1997), Oxidative stress causes coral bleaching during exposure to elevated temperatures, *Coral Reefs*, *16*(3), 187–192.

Liu, G., A. E. Strong, and W. Skirving (2003), Remote sensing of sea surface temperature during 2002 Barrier Reef coral bleaching, *EOS, Transactions, American Geophysical Union*, *84*(15), 137–144..

Liu, G., A. E. Strong, W. Skirving, and F. Arzayus (2005), Overview of NOAA coral reef watch program's near-real time satellite global coral bleaching monitoring activities, *Proc. 10th Int. Coral Reef Symp., Okinawa, Japan, 2004*, *1*, 1783–1793.

Lowe, R. J., J. L. Falter, S. G. Monismith, and M. J. Atkinson (2009), A numerical study of circulation in a coastal reef-lagoon system, *J. Geophys. Res.*, *114*, C06022, doi:10.1029/2008JC005081.

Lowe, R. J., C. Hart, and C. B. Pattiaratchi (2010), Morphological constraints to wave-driven circulation in coastal reef-lagoon systems: A numerical study, *J. Geophys. Res.*, *115*, C09021, doi:10.1029/2009JC005753.

Maina, J., V. Venus, M. R. McClanahan, and M. Ateweberhan (2008), Modelling susceptibility of coral reefs to environmental stress using remote sensing data and GIS models, *Ecol. Modell.*, *212*(3-4), 180–199, doi:10.1016/J.ECOLMODEL.2007.10.033.

Manzello, D. P., R. Berkelmans, and J. C. Hendee (2007), Coral bleaching indices and thresholds for the Florida Reef Tract, Bahamas, and St.

Croix, US Virgin Islands, *Mar. Pollut. Bull.*, *54*(12), 1923–1931, doi:10.1016/J.MARPOLBUL.2007.08.009.

Maynard, J. A., et al. (2008), ReefTemp: An interactive monitoring system for coral bleaching using high-resolution SST and improved stress predictors, *Geophys. Res. Lett.*, *35*(5), L05603, doi:10.1029/2007GL032175.

McCabe, R. M., P. Estrade, J. H. Middleton, W. K. Melville, M. Roughan, and L. Lenain (2010), Temperature variability in a shallow, tidally isolated coral reef lagoon, *J. Geophys. Res.*, *115*, C12011, doi:10.1029/2009JC006023.

McClanahan, T. R., M. Ateweberhan, C. R. Sebastian, N. A. J. Graham, S. K. Wilson, J. H. Bruggemann, and M. M. M. Guillaume (2007), Predictability of coral bleaching from synoptic satellite and in situ temperature observations, *Coral Reefs*, *26*(3), 695–701, doi:10.1007/S00338-006-0193-7.

Mellor, G. (2003), The three-dimensional current and surface wave equations, *J. Phys. Oceanogr.*, *33*(9), 1978–1989.

Miller, M. W., G. A. Piniak, and D. E. Williams (2011), Coral mass bleaching and reef temperatures at Navassa Island, 2006, *Estuarine Coastal Shelf Sci.*, *91*(1), 42–50, doi:10.1016/J.ECSS.2010.10.005.

Monismith, S. G., A. Genin, M. A. Reidenbach, G. Yahel, and J. R. Koseff (2006), Thermally driven exchanges between a coral reef and the adjoining ocean, *J. Phys. Oceanogr.*, *36*(7), 1332–1347.

Moore, J. A. Y., et al. (2012), Unprecendented mass bleaching and loss of coral across 12° of Latitude in Western Australia in 2010-11, *Plos One*, *7*(12), doi:10.1371/JOURNAL.PONE.0051807.

Mumby, P. J., J. R. M. Chisholm, A. J. Edwards, S. Andrefouet, and J. Jaubert (2001), Cloudy weather may have saved Society Island reef corals during the 1998 ENSO event, *Mar. Ecol. Prog. Ser.*, *222*, 209–216, doi:10.3354/MEPS222209.

Nadaoka, K., Y. Nihei, R. Kumano, T. Yokobori, T. Omija, and K. Wakaki (2001), A field observation on hydrodynamic and thermal environments of a fringing reef at Ishigaki Island under typhoon and normal atmospheric conditions, *Coral Reefs*, *20*(4), 387–398.

Niller, P. P. (1975), Deepening of the wind-mixed layer, *J. Mar. Res.*, *33*, 405–422.

Obura, D. O. (2005), Resilience and climate change: Lessons from coral reefs and bleaching in the Western Indian Ocean, *Estuarine Coastal Shelf Sci.*, *63*(3), 353–372, doi:10.1016/J.ECSS.2004.11.010.

Pearce, A. F., and M. Feng (2012), The rise and fall of the ''marine heat wave'' off Western Australia during the summer, *J. Mar. Syst.*, *111-112*, 139–156, doi:10.1016/J.JMARSYS.2012.10.009.

Reynolds, R. W., T. M. Smith, C. Liu, D. B. Chelton, K. S. Casey, and M. G. Schlax (2007), Daily high-resolution-blended analyses for sea surface temperature, *J. Clim.*, *20*(22), 5473–5496, doi:10.1175/2007JCLI1824.1.

Riegl, B., and W. E. Piller (2003), Possible refugia for reefs in times of environmental stress, *Int. J. Earth Sci.*, *92*(4), 520–531, doi:10.1007/S00531-003-0328-9.

Saha, S., et al. (2010), The NCEP climate forecast system reanalysis, *Bull. Am. Meteorol. Soc.*, *91*(8), 1015–1057, doi:10.1175/2010BAMS3001.1.

Sammarco, P. W., A. Winter, and J. C. Stewart (2006), Coefficient of variation of sea surface temperature (SST) as an indicator of coral bleaching, *Mar. Biol.*, *149*(6), 1337–1344, doi:10.1007/S00227-006-0318-0.

Shchepetkin, A. F., and J. C. McWilliams (2005), The regional oceanic modeling system (ROMS): A split-explicit, free-surface, topography-following-coordinate oceanic model, *Ocean Modell.*, *9*(4), 347–404, doi:10.1016/J.OCEMOD.2004.08.002.

Sheppard, C. R. C. (2003), Predicted recurrences of mass coral mortality in the Indian Ocean, *Nature*, *425*(6955), 294–297.

Simpson, C. J., J. L. Cary, and R. J. Masini (1993), Destruction of corals and other reef animals by coral spawn slicks on Ningaloo Reef, Western Australia, *Coral Reefs*, *12*, 185–191.

Smith, N. P. (2001), Weather and hydrographic conditions associated with coral bleaching: Lee Stocking Island, Bahamas, *Coral Reefs*, *20*(4), 415–422.

Smith, R. L., A. Huyer, J. S. Godfrey, and J. A. Church (1991), The Leeuwin Current off Western Australia, 1986–1987, *J. Phys. Oceanogr.*, *21*(2), 323–345.

Spalding, M. (2009), Detecting and monitoring coral bleaching events, in *Coral Bleaching: Patterns, Processes, Causes and Consequences*, edited by M. J. H. van Oppen and J. M. Lough, pp. 69–82, Springer, Berlin.

Strong, A., G. Liu, W. Skirving, and C. M. Eakin (2011), NOAA's Coral Reef Watch program from satellite observations, *Ann. GIS*, *17*(2), 83–92, doi:10.1080/19475683.2011.576266.

Tolman, H. L., and D. Chalikov (1996), Source terms in a third-generation wind wave model, *J. Phys. Oceanogr.*, *26*(11), 2497–2518.

Tolman, H. L., B. Balasubramaniyan, L. D. Burroughs, D. V. Chalikov, Y. Y. Chao, H. S. Chen, and V. M. Gerald (2002), Development and implementation of wind-generated ocean surface wave models at NCEP, *Weather Forecast*, *17*(2), 311–333.

Ware, J. R., D. G. Fautin, and R. W. Buddemeier (1996), Patterns of coral bleaching: modeling the adaptive bleaching hypothesis, *Ecol. Modell.*, *84*(1-3), 199–214.

Weeks, S. J., K. R. N. Anthony, A. Bakun, G. C. Feldman, and O. Hoegh-Guldberg (2008), Improved predictions of coral bleaching using seasonal baselines and higher spatial resolution, *Limnol. Oceanogr.*, *53*(4), 1369–1375, doi:10.4319/LO.2008.53.4.1369.

Wells, J. R., J. P. Fram, and G. Pawlak (2012), Solar warming of near-bottom water over a fringing reef, *J. Mar. Res.*, *70*, 641–660.

West, J. M., and R. V. Salm (2003), Resistance and resilience to coral bleaching: Implications for coral reef conservation and management, *Conserv. Biol.*, *17*(4), 956–967, doi:10.1046/J.1523–1739.2003.02055.X.

Wooldridge, S., and T. Done (2004), Learning to predict large-scale coral bleaching from past events: A Bayesian approach using remotely sensed data, in-situ data, and environmental proxies, *Coral Reefs*, *23*(1), 96–108, doi:10.1007/S00338-003-0361-Y.

Xu, J., R. Lowe, G. Ivey, C. Pattiaratchi, N. L. Jones, and R. Brinkman (2013), Dynamics of the summer shelf circulation and transient upwelling off Ningaloo Reef Western Australia, *J. Geophys. Res.*, *118*, 1099–1125, doi:10.1002/JGRC.20098.

Yee, S. H., D. L. Santavy, and M. G. Barron (2008), Comparing environmental influences on coral bleaching across and within species using clustered binomial regression, *Ecol. Modell.*, *218*(1-2), 162–174, doi:10.1016/J.ECOLMODEL.2008.06.037.

Zhang, Z., R. J. Lowe, J. L. Falter, and G. N. Ivey (2011), A numerical model of wave- and current-driven nutrient uptake by coral reef communities, *Ecol. Modell.*, *222*, 1456–1470, doi:10.1016/J.ECOLMODEL.2011.01.014.

Zhang, Z., J. Falter, R. Lowe, and G. Ivey (2012), The combined influence of hydrodynamic forcing and calcification on the spatial distribution of alkalinity in a coral reef system, *J. Geophys. Res.*, *117*, C04034, doi:10.1029/2011JC007603.